Thermo-Hydrological and Chemical (THC) Modeling to Support Field Test Design

Fuel Cycle Research & Development

Prepared for
U.S. Department of Energy
Used Fuel Disposition Campaign
Milestone M4FT-14LA0818064

P.H. Stauffer, A.B. Jordan, D.A. Harp, G.A. Zyvoloski, H. Boukhalfa , F.A. Caporuscio, T.A. Miller, B.A. Robinson
Los Alamos National Laboratory
September 30, 2014
Los Alamos National Laboratory Document LA-UR-14-27548

EXECUTIVE SUMMARY

This report summarizes ongoing efforts to simulate coupled thermal-hydrological-chemical (THC) processes occurring within a hypothetical high-level waste (HLW) repository in bedded salt. The report includes work completed since the last project deliverable, "Coupled model for heat and water transport in a high level waste repository in salt", a Level 2 milestone submitted to DOE in September 2013 (Stauffer et al., 2013).

Since the last deliverable, there have been code updates to improve the integration of the salt module with the pre-existing code and development of quality assurance (QA) tests of constitutive functions and precipitation/dissolution reactions. Simulations of bench-scale experiments, both historical and currently in the planning stages have been performed. Additional simulations have also been performed on the drift-scale model that incorporate new processes, such as an evaporation function to estimate water vapor removal from the crushed salt backfill and isotopic fractionation of water isotopes. Finally, a draft of a journal paper on the importance of clay dehydration on water availability is included as Appendix I.

THERMO-HYDROLOGICAL AND CHEMICAL (THC) MODELING TO SUPPORT FIELD TEST DESIGN

Introduction: Numerical model development (Oct 2013 – Sept 2014).

During the 2014 fiscal year, code development on FEHM continued, focusing on four main areas:

- 2013 code developments were brought into the current version of the code (FEHM 3.2). The code realignment work was necessary because the original salt modifications were added to version 3.1 beginning in 2012. To provide more user utility to the code, a salt control driver was added. This involved re-coding how functions such as dissolution/precipitation, clay dehydration, and constitutive relationships specific to salt are called from within FEHM. Additionally, new input functionality was added to FEHM with documentation explaining the input parameters.
- Quality assurance (QA) problems have been implemented to provide a check on the accuracy of both constitutive functions (e.g., heat transfer) and precipitation/dissolution reactions.
- Simulations were designed to recreate a previously published experiment that demonstrated the formation of a multiphase heat-pipe in granular salt.
- Simulations are presented that capture planned laboratory scale experiments.
- Simulations with new processes were performed in support of a large scale thermal test (LSTT) that is planned for implementation in the underground at the Waste Isolation Pilot Plant. In particular, a model for evaporation was added to the crushed salt backfill and isotopic tracers were simulated in the drift-scale model. Simulations were also performed to test the effect of cool-down of the heaters after the two-year heated test period.

This report is divided into five main sections. The first section describes code developments that have been added into the latest version of the LANL-developed porous flow/reactive transport simulator (FEHM). The second section provides the new QA tests that have been implemented. The third section describes simulations that recreate an experiment in which a heat-pipe was formed in granular salt (Olivella et al., 2011), confirming the hypothesis in our 2013 report that this mechanism could be potentially important for understanding heat generating waste in salt repositories. The fourth section includes a description of simulations of bench scale testing that will be done before the full in-drift thermal testing, and the fifth section describes LSTT simulations with a focus on new simulations and capabilities added since the previous milestone (Stauffer et al., 2013). Appendix I is a draft journal article on clay dehydration in FEHM. This process was implemented in the previous fiscal year and discussed in Stauffer et al. (2013) and is expanded in this draft publication.

1. FEHM Modifications

1.1 Code Control Module

A new controller module (saltctr.f) was created to manage simulations with salt. The salt controller was implemented for three primary reasons. First, we needed to consolidate the salt-related software modifications (dissolution/precipitation, constitutive laws, clay dehydration, etc) into one location so that those modifications could be merged with the primary FEHM software suite and allow a platform for future software development. Second, the new controller allows one to more easily (via user input) isolate different salt capabilities to be tested separately to assess individual modification importance and sensitivity. Third, the controller now allows the testing of numerical algorithms associated with the averaging and temporal updating of the highly nonlinear salt-related physics. This new module was tested to insure that the resulting code produced the same numerical output on a set of quality assurance problems designed to ensure that the salt functions are working properly. The newly designed input description is provided in Section 2.2 and a description of source code that was changed is included in Section 2.3.

Key additions to capability include:

1. The ability to run salt simulations with a variety of combinations of water vapor formulations with vapor pressure lowering with different salt concentrations and capillary pressure vapor pressure lowering.
2. The option to initialize gridblocks to saturation temperature at total fluid pressure or total fluid pressure at saturation temperature. The partial pressure of air in these conditions was set to a prescribed small number.
3. Improved numerical performance with temporal averaging of porosities and permeabilities. This simple change allowed significantly smaller porosities to be reached in a simulation while maintaining large time steps. It also was the difference between simulations finishing and not finishing for some parameter combinations.

1.2 Newly designed input for the salt controller

The input structure for the SALT module is similar to that of CO_2 and stress modules. That is, it makes use of sub-keywords within the SALT input section. This module allows input that is also available from other keywords (*ppor*, *adif*, *vapl*) but is logically included here as well.

KEYWORD "saltppor" Keyword specifying type of porosity compressibility model

Group 1 - IPOROS (only IPOROS = 6 or 7 allowed)

Group 2- JA, JB, JC, POR1 ,POR2 ,POR3, POR4 (1 parameter entered for IPOROS = 6, 4 parameters entered for IPOROS = 7)

An warning message in written to the output file and the ".err" file if a salt porosity model is not entered.

KEYWORD "saltvcon"

Only one thermal conductivity model (4) is implemented for salt in the saltctr. It is based on the thermal conductivity for crushed salt (Bechthold et al, 2004).

Group 1 - IVCON(I), VC1F(I), VC2F(I) , VC3F(I), VC4F(I), VC5F(I), VC6F(I), VC7F(I), VC8F(I)

Group 2- JA, JB, JC, IVCND

Input Variable	Format	Description
IVCON(I)	integer	model type IVCON(I) = 4 (only salt model available)
VC1F(I)	real	reference temperature (C)
VC2F(I)	real	porosity-related used in Bechthold equation
VC3F(I)	real	Coefficient of 4th order term in Bechthold equation
VC4F(I)	real	Coefficient of 3rd order term in Bechthold equation
VC5F(I)	real	Coefficient of 2nd order term in Bechthold equation
VC6F(I)	real	Coefficient of 1st order term in Bechthold equation
VC7F(I)	real	Constant term in Bechthold equation
VC8F(I)	real	Power law term in Bechthold equation
IVCND	integer	model number to apply to nodes

An warning message is written to the output file and the ".err" file if a salt thermal conductivity model is not entered.

KEYWORD "saltden"

KEYWORD "saltadif"

Group 1 - TORT

The appropriate diffusion models are TORT = 333 and TORT = 666 and are based on the Millington Quirk model as programmed originally by Pruess(ref?). If other models are used, a warning message is written to the output file and the ".err" file.

KEYWORD "saltvapr"

Group 1 - IVAPRSALT

IVAPRSALT - identifies the vapor pressure lowering model

Reference: Sparrow (2003) Desalination

Note: The Sparrow formulation has no capillary vapor pressure lowering.

Input Variable	Format	Description
IVAPRSALT	integer	IVAPRSALT = 0 - traditional FEHM h2o vapor pressure fit with vapor pressure no lowering
IVAPRSALT	integer	IVAPRSALT = 1 - Sparrow vapor pressure model with no salt
IVAPRSALT	integer	IVAPRSALT =2 - Sparrow vapor pressure model with salt
IVAPRSALT	integer	IVAPRSALT =3 - Sparrow vapor pressure model

with salt and capillary vapor pressure lowering (not yet implemented) IVAPRSALT integer IVAPRSALT =4 - traditional FEHM vapor pressure model with capillary vapor pressure lowering IVAPRSALT integer IVAPRSALT =5 - traditional FEHM vapor pressure model with salt and no capillary vapor pressure lowering IVAPRSALT integer IVAPRSALT =6 - traditional FEHM vapor pressure model with salt and capillary vapor pressure lowering

KEYWORD "saltnum"
This keyword manages the updating of the nonlinear salt related variables
Group 1 - ACTION, VALUE

Input Variable	Format	Description
ACTION	character	Salt process to be modified ACTION = " permavg" - average permeability after every *tracer* timestep ACTION = " poravg" - average porosity after every *tracer* timestep ACTION = " pormin" - set minimum porosity
VALUE	real	parameter value related to process ACTION = " permavg", VALUE = 1-use new time step permeability VALUE = 0-use old time step permeability VALUE = 0.5-use average permeability ACTION = " poravg", VALUE = 1-use new time step porosity VALUE = 0-use old time step porosity VALUE = 0.5-use average porosity ACTION = " pormin", VALUE = minimum porosity for ppor model 7

KEYWORD "saltend"

1.3 Description of source code changes

saltctr.f- new controller subroutine for managing salt simulations

co2ctr.f- modified input to allow inputted temperature to be changed to saturation pressure at total pressure (setting air partial pressure to small value) and to change inputted temperature to saturated water vapor temperature at total pressure (air partial pressure to small value)

csolve.f - added call to saltctr to manage porosity and permeability changes

fehmn_pcx.f- removed call to porosi for salt controlled porosity update (was only for salt porosity models anyway)

comai.f- added more global variables required for the salt controller

porosi.f- added call to saltctr to manage porosity and permeability changes and moved salt-related printout to saltctr.

wrtout.f- added call to saltctr for salt output

outbnd.f- added call for new salt output to be printed when variables go out-of-bounds.

comdi.f- added another permeability array for last tracer timestep for permeability averaging

dvacalc.f- added coding to prevent a divide-by-zero for variable dvas(). *Don't see where dvas() is used.*

thrmwc.f- added call to saltctr.f for vapor pressure of water

input.f- modified for the inclusion of SALT module (saltctr.f)

allocmem.f- added memory allocation for salt variables

startup.f- added concen call to initialize anl for first flow timestep when using cden

1.4 Description of salt algorithm

This section describes the numerical flow of the newly designed salt controller.

At timestep *n* and simulation time *days*:

1. Solve coupled equations for P,T, P_a, and S.
2. Save the internodal flowrates for liquid and vapor phases.
3. Solve the tracer transport equations from timestep *n-1* to *n* (time = *days*). The transport equations are solved at smaller timesteps than the flow equation.
    a. At every transport equation evaluate the chemical reactions and quantify precipitation or dissolution of salt and change the porosity.
    b. From the porosity change, evaluate the permeability change
    c.
4. Update flow equation properties, Go step 1.

1.5 Improved code for calculation of porosity change

During the 2014 FY (Oct 2013 – Sept 2014) a modification to FEHM was made to improve calculation of porosity change. The previous version of the code used changes in solid concentration (moles of solid/ mass of solid) during a tracer time step to calculate porosity change. The improved algorithm uses the time rate of change of the number of moles of the solid phase to calculate porosity change. The new code logic is simpler in that it uses a previously calculated value to determine porosity change. Differences between the methods are small and are shown in figure 1.5_1.
This figure shows the porosity change (old – new) after 2 years of simulated heating for a case with an initial run of mine salt moisture content of 1.25% and 5x750W heaters.

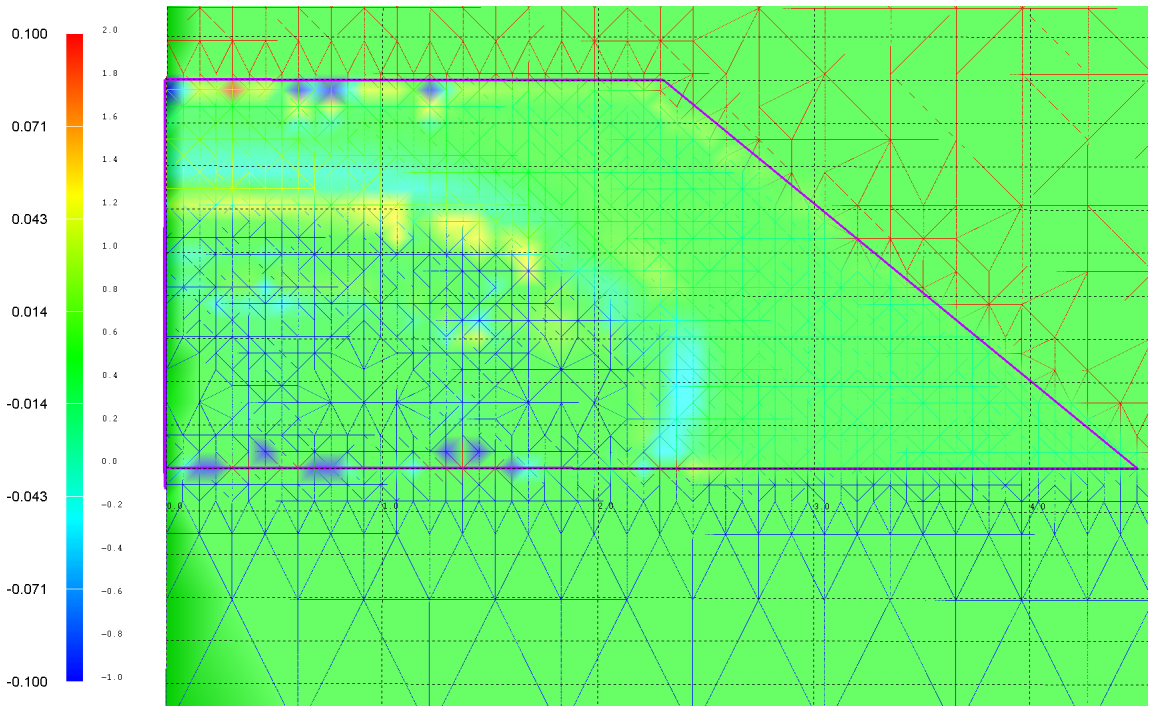

Figure 2.1_2 Difference in porosity after code modification (Old – New)

In the following code, the comment lines at the top (blue) are notes on the code changes. The red commented out section of FORTRAN code represents the old version while the green text at the bottom is the new algorithm. One complication in understanding the implementation is that FEHM separates the density of the solid component of the porous media from the density of chemical reactions that form solids. In the salt repository simulations, these densities are assumed to be the same (i.e. the tracer is the solid matrix).

```
c PHS and DHR 7/31/13  Changed to expression:
c      delta por = delta(mol/kg rock)*rock density(kg rock/m3 rock)*
c           *(1-porosity) (m3 rock/m3 tot)
```

```
c          *molecular weight(kg salt/mol)/ salt grain density (kg salt/m3 salt)
c     = delat m3 salt /m3 total.
c
c PHS 8/1/13  Also added call to porosi and reset an to anlo to maintain
c          constant mol/kg of salt.
c PHS 8/2/13  Added a throttle to stop the porosity loss below 1e-3 when porosity
c          is decreasing (ps_delta_rxn -VE)
c PHS 11/20/13 Changing to rc(mi) to drive ps_delta_rxn.  sx1 = cell volume
```

Old code based on change in solid concentration. an(ja) and anlo(ja) are the current and previous time step values of concentration of the solid (mol salt/kg rock), mw_mineral(im) is the molecular weight of the mineral, rho_mineral(im) is the tracer mineral density, denr(i) is the solid rock density, and ps(i) is the cell porosity.

```
c               ps_delta = -((an(ja)-anlo(ja))*denr(i)*
c    &               (1-ps(i))*mw_mineral(im)/rho_mineral(im))
```

New code based on rate of change of solid moles (mol/time). dtotc is the tracer time step length, and sx1 is the volume of the cell.

```
               ps_delta_rxn(i) = rc(ja)*dtotc*mw_mineral(im)
     &              /rho_mineral(im)
               ps_delta_rxn(i) = ps_delta_rxn(i)/sx1(i)
```

2. Quality Assurance (QA) examples

Complex coupled processes require QA test problems that isolate individual processes to ensure correct code execution. In the following sections we describe two examples of such QA test that have been implemented into the FEHM test suite (REF fehm.lanl.gov).

2.1 Dissolution/precipitation QA test

To isolate the process of dissolution/precipitation, a simple model has been designed that allows hand calculation of porosity change to which numerical results can be compared. This is not as straight forward a task as it might appear. In the system that we are work with, there are many coupled processes that impact the movement of both liquid water and water vapor (Stauffer et al, 2014). As heat causes water to evaporate, capillary suction increases and leads to high pressure gradients in the direction of the heating. Water vapor pressure above a cell that has completely dried out can become less than 100% saturated leading to reverse vapor gradients moving water vapor toward dry cells. By adjusting the capillary function through making the residual saturation very high (99.9%) we were able to stop the return flow of water to the dry end of a 1-D numerical mesh, allowing exact calculation of the initial mass of dissolved salt. Using the density and molecular weight of salt, porosity change at the node on the hot end can then be calculated exactly.

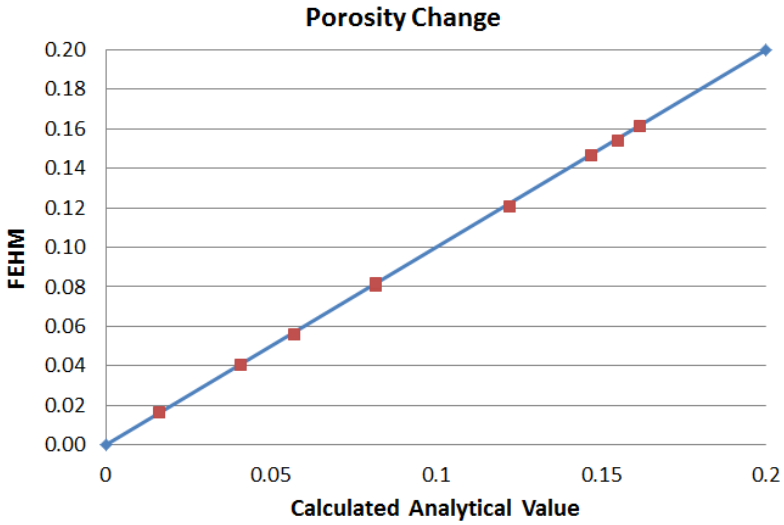

Figure 2.1_1 FEHM versus analytical porosity change for salt precipitation during evaporation

2.2 Dissolution/precipitation QA test

To ensure isotopic fractionation is working correctly, a simulation was created using water as a tracer of itself. This QA algorithm was originally developed for tritium analysis (H^3) at Los Alamos and atmospheric tracer transport simulations (H^3, Deuterium (D), and O^{16} and O^{18}) at the Nevada Test Site (Kwicklis et al., 2006). Results below (Figure 2.2_1) show water at 55.55 mol/kg in a 6 node problem. When the code is working H_2O^{16} water does not fractionate from itself. The right side of the figure shows the behavior before the fix. The top row is water as its own tracer, the middle for HDO with a fractionation factor relative to water of h*=0.922, and the bottom row H_2O^{18} with h*=0.974 relative to water, with the Henry's partition coefficient of H_2O^{16} water being simply 1.0*water vapor pressure.

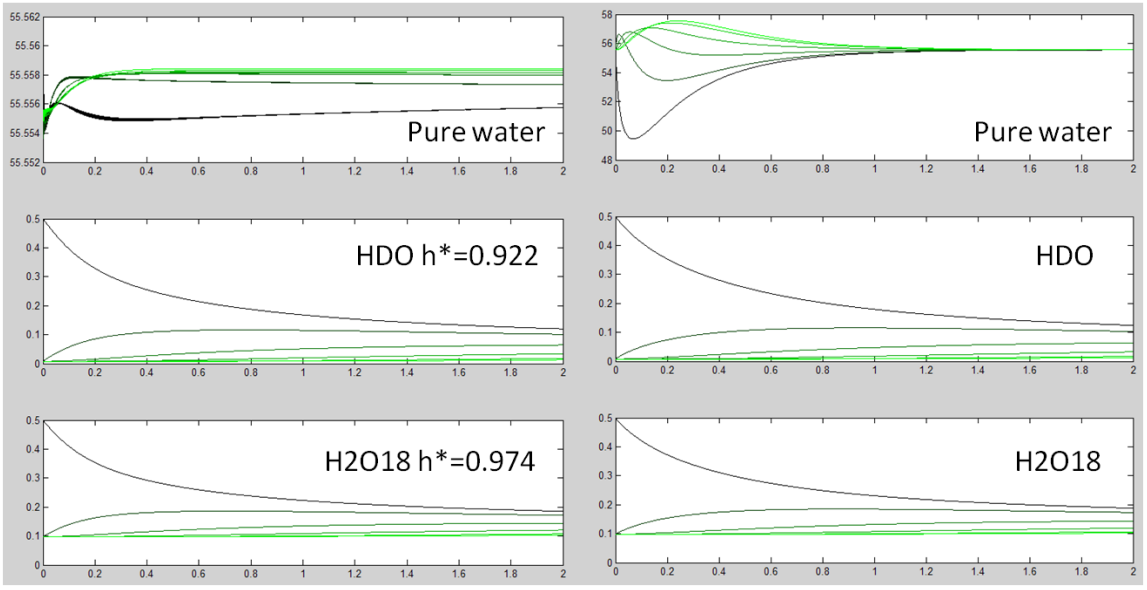

Figure 2.2_1 QA test results for FEHM. The left side shows results after the correct diffusion function was coded for the salt problem.

2.3 Thermal conductivity QA test

A test for the variable thermal conductivity model in FEHM was constructed. This test compares empirically generated thermal conductivity functions of both run of mine (RoM) salt and intact salt of varying porosity and saturation to those computed within the code. Run of mine salt is roughly crushed during mining operations. The equations for variable thermal conductivity are reported in Stauffer et al. (2013). Output from the test is reported in the validation report as:

Salt Variable Conductivity Test
Comparison of Salt Conductivity Model to Emperical Function Results

Test Case	Maximum	Error Maximum	% Error RMS Error
Model intact	4.320E-05	9.014E-04	2.590E-06
Model crushed	4.560E-05	3.669E-03	1.043E-05

3. Simulation of an existing heat-pipe experiment

Our investigations focus on a generic bedded salt repository design known as the in-drift disposal concept. Canisters of HLW are emplaced on the floor after excavation of the room, and backfilled with crushed RoM salt. There are complex and strongly coupled thermal, hydrological, chemical, and mechanical processes that take place when heated waste is added to this system.

If the temperature of the waste exceeds the boiling point of brine, water will evaporate and migrate in the vapor phase before recondensing beyond the boiling front. Depending on a complex set of variables, a heat pipe may be established in the crushed salt (Figure 3_1). In a heat pipe, free water is vaporized in the boiling region, advects and diffuses along concentration gradients to the cooler regions where it recondenses, and some of the liquid flows back toward the heat source by gravity flow and along capillary pressure gradients where it is boiled off and the cycle is repeated. The replenishing fluid is saturated brine; when boiled off, it deposits a layer of salt around the heater. This leads to the build-up of a low-porosity "rind" while the heat pipe is sustained.

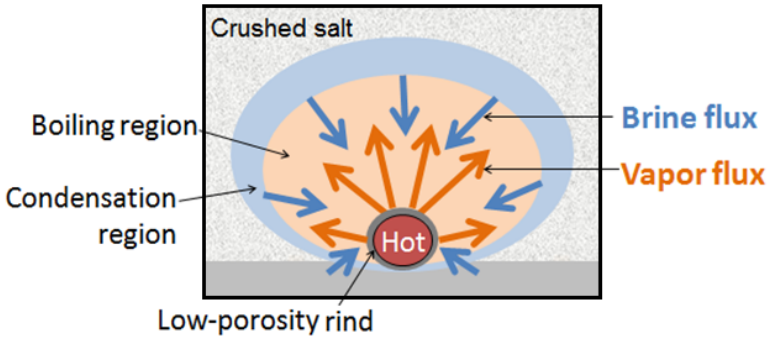

Figure 3_1. Heat pipe in salt.

To our knowledge, the only published experimental work on heat pipes in crushed salt is the laboratory work of Olivella et al. (2011). In the experiment by Olivella et al., a heat pipe was established in a 5 cm by 10 cm cylindrical apparatus with fixed temperature plates on the cylinder ends and a closed system for mass transport. Porosity change was observed along the length of the cylinder as expected for a heat pipe, with dissolution at the cold end where water vapor is condensing and buildup of a low-porosity rind at the hot end where water is evaporating. Destructive testing of the system at various times (7, 15, 30, and 65 days) determined the spatial and temporal pattern of porosity change and saturation. The authors also compared model results to the experiments. The experimental results were well-matched by the numerical model CODE-BRIGHT for the same scenario (Olivella et al., 2011). Their work also produced a surprising result, which is that the final state of the system was relatively insensitive to initial saturation, a finding that contradicts longer-term FEHM drift-scale model results (2 years) but agrees with some bench-scale modeled scenarios using FEHM. Our work is intended to confirm the results of Olivella et al. in a somewhat more realistic scaled system with controlled airflow allowed and more space around the heater for RoM backfill.

3.1 FEHM simulations of the Olivella (2011) experiment

FEHM was set up to closely match the Olivella simulations. A 0.1 m 1-D mesh with 40% saturation and 40% porosity was built. A retention curve with alpha = 1.43 and n = 2.3 is used. Variable thermal conductivity for RoM salt and vapor diffusion as a function of porosity and saturation is used (Millington/Quirk). A permeability function similar to Olivella is used (2.7e-13 to 2.7e-12 m^2). Figure 3.1_2 shows FEHM results for a 65 day simulation with heating of 85C on one end of the 1-D domain and 5C on the other. Figure 3.1_2 shows the results of the Olivella experiment for comparison. The trend in the FEHM simulations is the same direction as the experiment; however we are under predicting the porosity increase on the cold end while over predicting the porosity decrease on the hot end. The conservation of salt in the FEHM simulation is precise to more than 4 significant figures, so the difference in the two results appears to be in the physical processes simulated versus the processes functioning in the experiment. Interestingly, Olivella's simulation of the experiment shows a decrease in porosity at the hot end to less than 0.1 in 65 days similar to the FEHM calculations. However, much larger porosity increase is calculated by Olivella for the cold end. Work is ongoing to understand the differences in these simulations and the experiment.

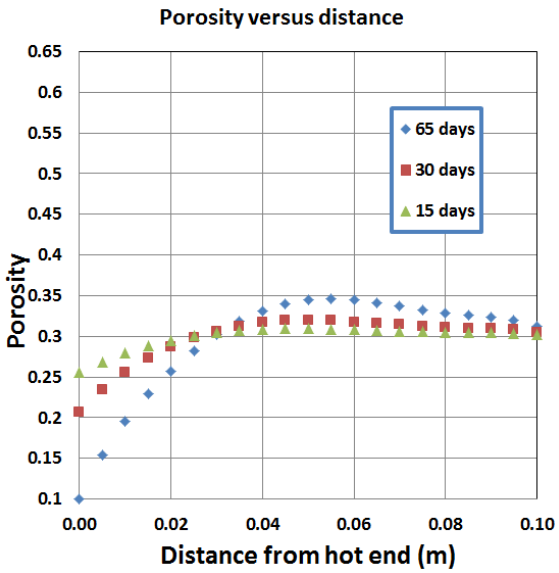

Figure 3.1_1 FEHM simulated porosity change.

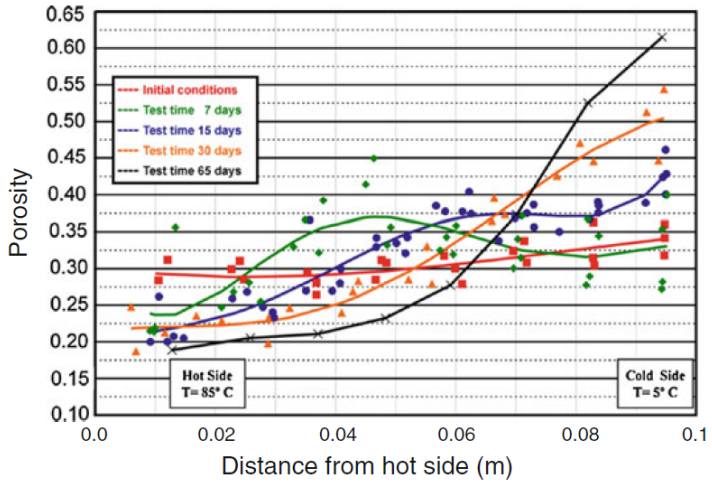

Figure 3.1_2 Olivella experimental porosity change

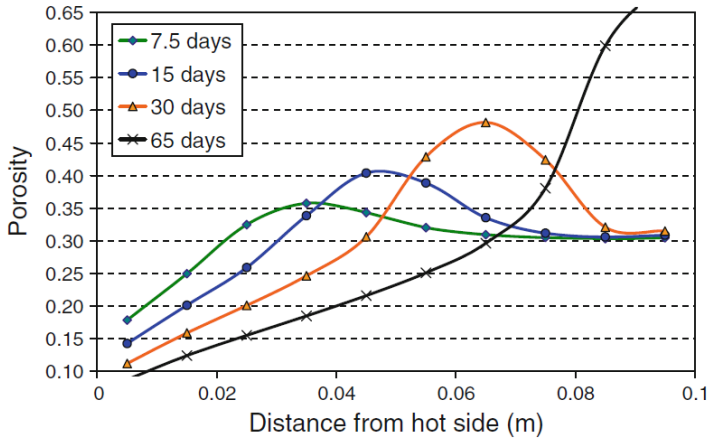

Figure 3.1_3 Olivella simulated porosity change

4. Laboratory-scale simulations

Models were also developed to test whether the heat-pipe results seen at the drift scale would likely be reproducible in the laboratory. Initial results indicate that it will be possible to see porosity change after only a few days of heating for a fairly simple setup. Modeling was performed for various designs, including a thin tank, a square tank, a rectangular tank; the heater was placed on the floor of the tank, or raised in the crushed salt pile; and the presence or absence of a saturated layer beneath the heater was considered. Models such as these will be used throughout the experimental design process to design the exact setup and predict the detectability and redistribution of tracers such as HDO, D_2O, and $H_2{}^{18}O$.

An example of one small-scale 3-D model is shown in Figure 4_1. In this case, a square tank of dimensions 0.3 by 0.3 m (1.0 by 1.0 ft) has a heating element elevated to 5 cm above the bottom of the tank. Elevating the heater provides additional insulation to heat loss from the bottom, unless the tank bottom is well-insulated. The initial porosity was 35% in the RoM salt and initial saturation was 5%. Temperature, saturation, and porosity at 1 and 5 days are shown in Figure 4_2. The porosity change around the heater would likely be observable in the laboratory.

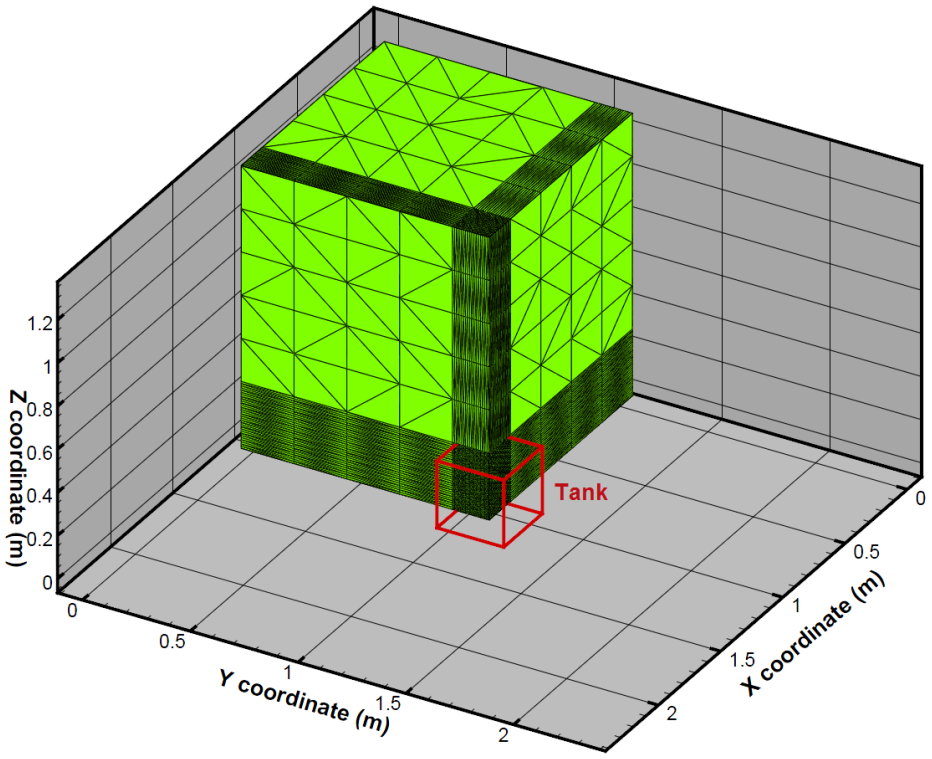

Figure 4_1 Cut-away showing one-quarter of the computational mesh for the laboratory-scale model with a 1 ft by 1 ft by 1 ft tank. Minimum mesh size was 1 cm in the tank, and maximum mesh size was 24.5 cm in the air.

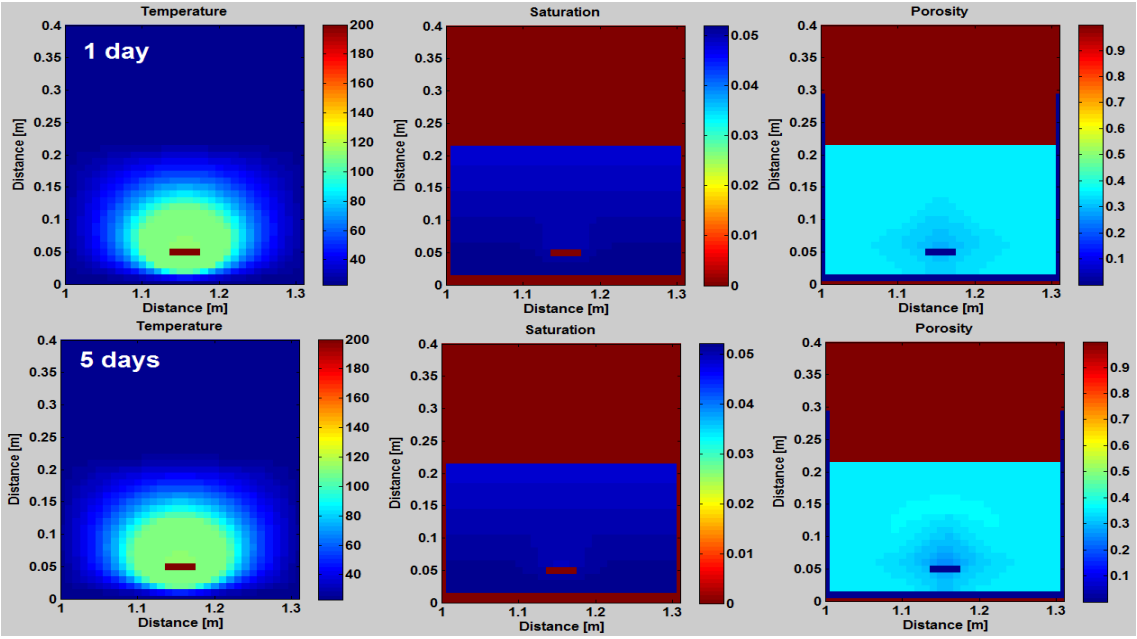

Figure 4_2 Model results (temperature, saturation, and porosity at 1 day and 5 days) for a 0.3 by 0.3 m (1.0 by 1.0 ft) open tank with salt to 20 cm height. The heater is elevated by 5 cm in the crushed salt.

Sensitivity studies can be quickly performed with the model to test different setups and design an experiment with high likelihood of heat pipe formation. For example, for a particular scenario, the effect of temperature, initial saturation, and maximum capillary suction are shown in Figure 4_3. This model is of a larger tank than the case above; dimensions were 40 cm by 80 cm by 20 cm. In this case, likely due to model assumptions and the setup chosen, initial saturation and maximum capillary suction have little effect on heat pipe vigor (extent of the 0.2 porosity contour), while temperature of the heater has a significant effect. The results below are preliminary; additional modeling will be performed in as part of the experimental design effort.

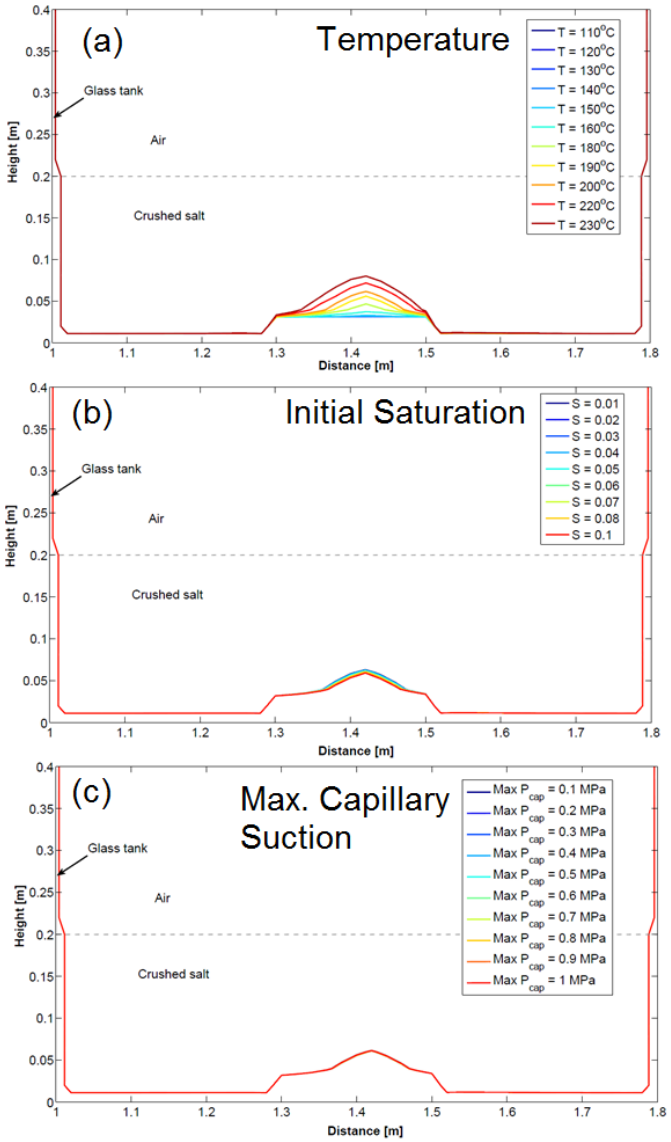

$\phi = 0.2$ *contours*

Figure 4_3. Effect of temperature, initial saturation, and maximum capillary suction on porosity (ϕ) after 5 days of heating. The $\phi = 0.2$ contours are shown. Initial porosity was 0.35.

5. Large scale thermal testing simulations

5.1 Previous drift-scale simulation results

FEHM modeling results at the drift scale suggest that a wide range of behavior (from extensive heat pipe activity to none) can occur in the RoM salt based on availability of both water and heat and the ability of water to move at low saturations (Stauffer et al., 2013). One of the primary indicators of a heat pipe is porosity change. In drift-scale simulations, porosity change from the initial 35% in the model is seen in Figure 5.1_1. In this case the only parameter varied was the heat load in the canisters. For increasing heat loads ranging from 250W to 750W in Figure 5.1_1, the porosity changes are significantly enhanced for higher heat loads and temperatures. In all cases there is little water flowing into the RoM salt from the damaged rock zone (DRZ), the

initial saturation of the RoM pile is 10%, and the maximum capillary suction in the RoM salt is 1.0 MPa. We define a metric for total porosity change as follows:

PC_{tot} = sum over all RoM nodes (abs(initial porosity – final porosity).

This metric sums both gains and losses to total porosity in a zone. In all simulations we restrict our porosity change to the RoM salt pile. For case A, this value is 0.16 m^3, for case B it is 0.46 m^3, while for case C PC_{tot} = 1.18 m^3. In all cases this value is positive implying porosity loss with time.

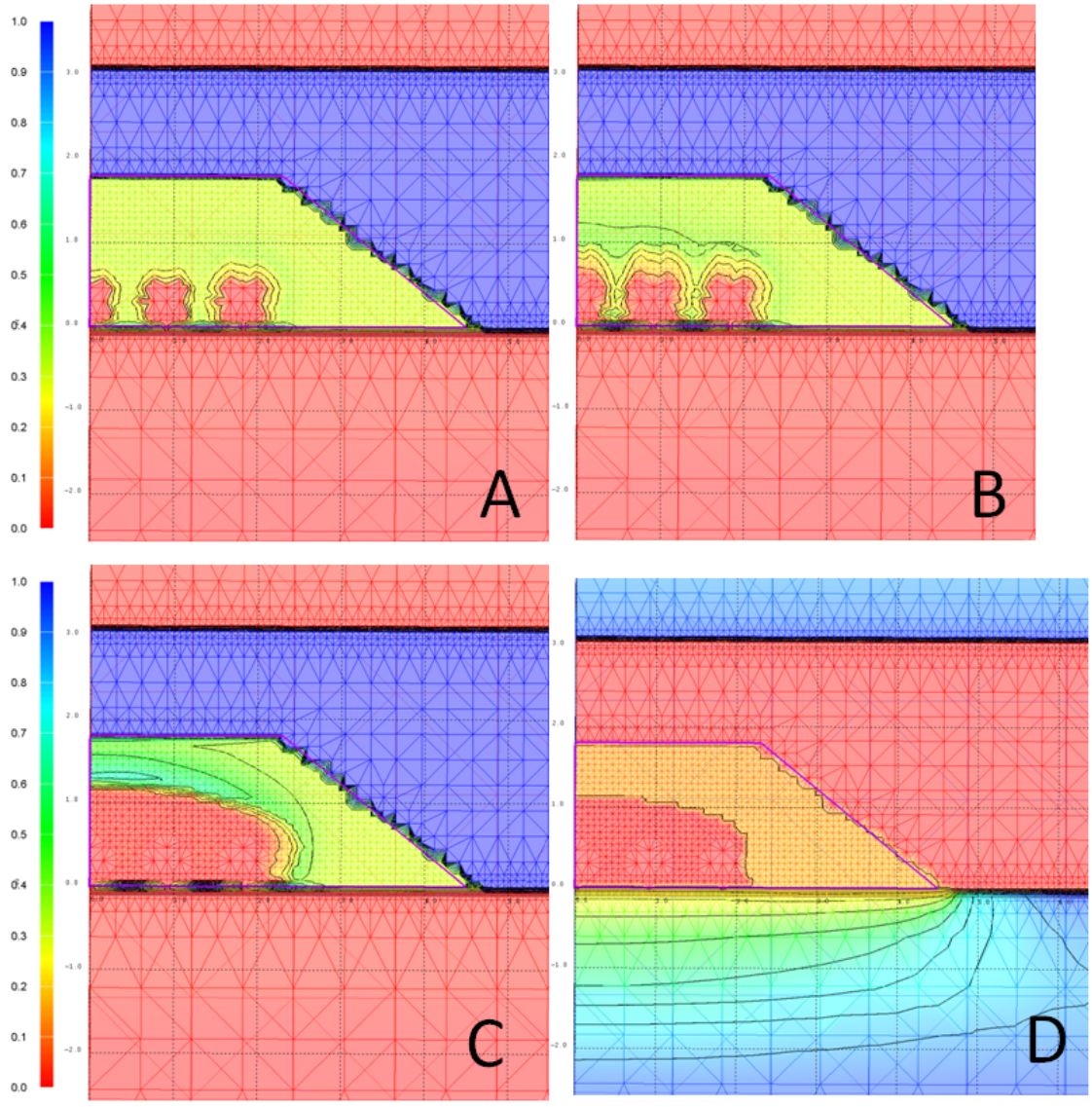

Figure 5.1-1: Porosity after 2 years of heating for A) 250W B) 500W and C) 750W per heater. D) Saturation corresponding to the porosity in C.

The large changes in porosity seen in the 750W case are caused by the heat pipe effect whereby purified water vapor is driven away from the heat source and saturated brine is pulled back towards the heat from wetter regions to the very dry region that develops around the heaters. Note that the model does not consolidate the crushed salt when porosities become very large in the condensation halo. The dry-out region can be seen in Figure 5.1_1D.

Other sets of simulations have demonstrated the impact of initial available water and capillary suction properties on porosity redistribution (Stauffer et al., 2013). Initial saturation in the crushed salt is an uncertain parameter, depending on many factors such as how long the RoM backfill has been allowed to sit in the ventilated repository before enclosing the waste. Additionally, it is extremely difficult to quantify the amount of water that will seep into the excavated drift; past brine flow investigations have produced extremely varied results (Kuhlman and Malama, 2013). For this reason, initial saturation was varied from 0.01 to 0.10 and the effect on the heat pipe was modeled. Very low saturation cases did not produce a heat pipe, even with clay dehydration added to the code to release water at appropriate temperatures for dehydration reactions. At some intermediate saturation, depending on clay content, a heat pipe becomes possible. There are large simulated temperature differences (40C) between the wet initial conditions that create a heat pipe and the other initial states that do not lead to heat pipe formation.

Capillary suction affects the available water in the RoM salt through interactions with the EDZ beneath the pile. With greater suction, more water can be pulled into the RoM salt, providing more drive for the heat pipe. Similarly, more suction allows the heat pipe to strengthen, as increased suction is more efficient at pulling saturated brine back towards the hot region. Varying from 0.1 MPa of maximum suction in the RoM salt to 0.5 MPa impacts the two year porosity distribution. The PC_{tot} for these cases is 0.29 m^3 and 0.38 m^3, respectively. In both cases the initial saturation is 5% with 750W canisters.

5.2 Cool-down simulations

In the following sections we describe results from a simulation of cool down following two years of heating for cases both with and without a heat-pipe. Figure 5.2_1 shows how the higher temperatures created without a heat-pipe asymptote to approximately the same values as those from the heat-pipe case within 40 days of the heat source being removed. This is largely due to the very high thermal conductivity of intact salt. In both cases, the highest temperatures in the simulations are found within the heaters (1 ft and 1.5 ft respectively). Temperatures at the RoM/heater interface for both cases are approximately 20 C lower than the maximum found within the heaters. By 30 days post test, temperatures in the drift should be manageable with gloves (<45C = 113 F).

Figure 5.2_2(A) shows change in saturation for the case with no heat pipe. Saturation increases on the floor while drainage occurs at the location of the boiling front where condensate allowed increased saturations while the heat source was active. Interestingly, for the heat-pipe case, the maximum saturation increase is seen between the simulated waste canisters (heaters) and also along the boiling front where water can move back into the very dry salt just below the boiling line. Because of the latent heat transfer, the boiling line lies higher in the pile on (A) which has retention characteristics chosen to limit flow at lower saturations. Thus, it can be seen that the

distribution of water and the long term temperature profiles within the RoM salt are a strong function of the ability of the salt to transport liquid water under relatively dry conditions (10% sat = 1.25 weight percent water).

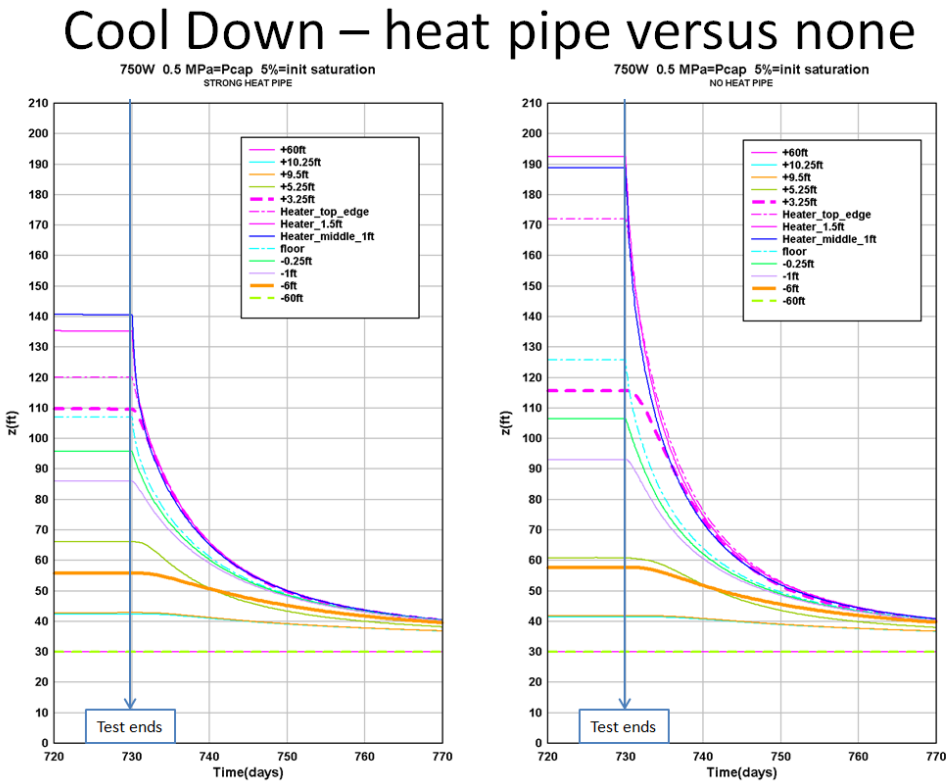

Figure 5.2_1 Cool down after 2 years of heating at 750W. A) Heat pipe and B) No Heat pipe

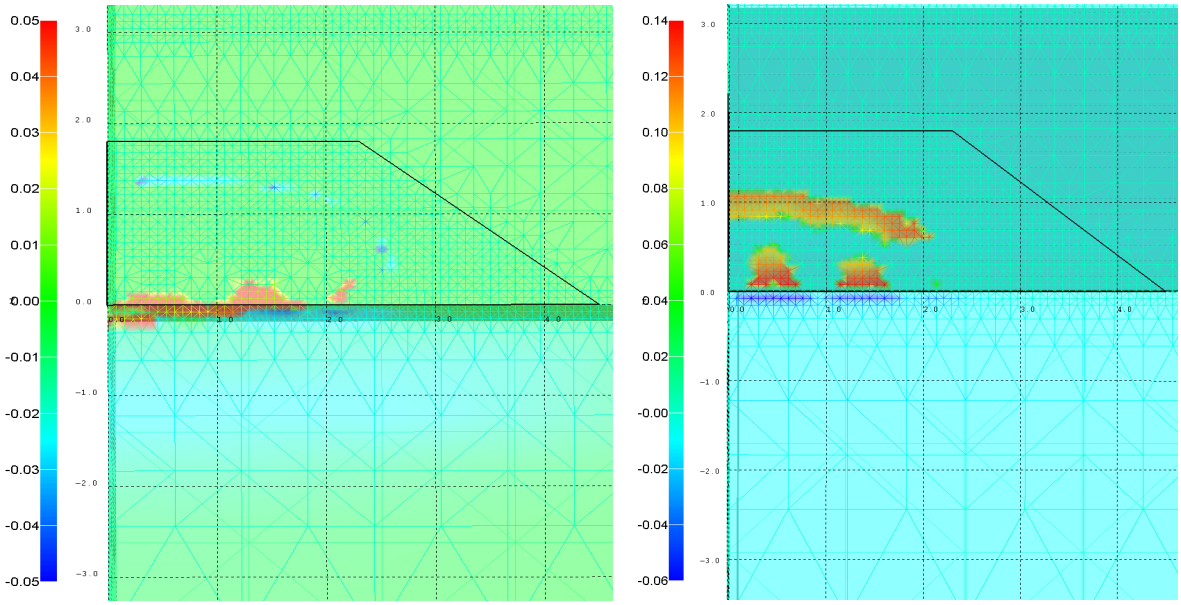

Figure 5.2_2 Change in saturation after 60 days of cool down from A) the case without a heat pipe and B) with a vigorous heat pipe. Red indicates higher final saturations.

5.3 Isotopic tracer simulations

Deuterium (D) and oxygen 18 (O^{18}) isotopes were simulated through the introduction of tracer into the RoM pile (Figure 5.3_1A). D naturally occurs at 156 ppm (0.0173 mol/kg water) while O^{18} naturally occurs at 2005 ppm or 0.111 mol/kg water. For D, fractionation between liquid and vapor is fairly high with an effective Henry's partition factor (dimensionless) at 20C of:

$$\text{D partition coefficient} = 0.92 * H_2{}^{16}O \text{ partition coefficient}$$

For O^{18}, the fractionation is lower:

$$O^{18} \text{ partition coefficient} = 0.99 * H_2{}^{16}O \text{ partition coefficient},$$

The $H_2{}^{16}O$ partition coefficient is defined by the water vapor pressure at a given temperature and brine salt concentration.

Fractionation through boiling without a spike may be sufficient to measure changes in concentration, as condensation will drop the concentration of D relative to H_2O and boiling will leave behind higher concentrations of D in the liquid. Post test sampling may be able to see the impacts of the boiling and condensation zones. Pure $H_2{}^{18}O$ water is 50 mol/kg and costs 245$/gram or 400$ for 2g. Pure D_2O water is 50 mol/kg, and costs 1200$/kg. Using this level of D, the tracer is acting as a bulk water tracer and will overwhelm traditional delta D analysis, but be quite robust in showing to where the system a spike has migrated.

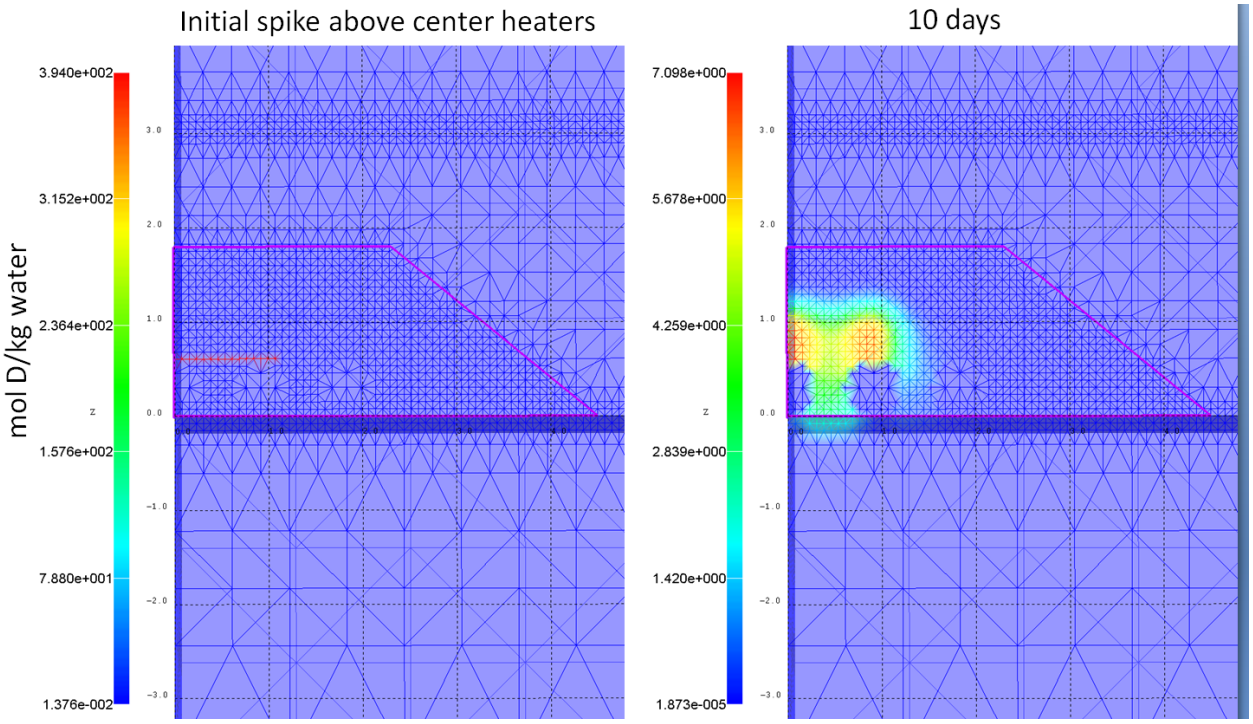

Figure 5.3_1 A) intial spike of deuterium (red line directly on top of the canisters and B) migration and dilution of deuterium after 10 days simulated time.

Figures 5.3_1 and 5.3_2 show results for migration of a spike of D after 10 days of simulated time. In both cases the canisters each produce 750W (in full 3D), the initial water content of the RoM salt is 1.25% (gravimetric), and the RoM suction at residual water content (0.625%) is 0.5 MPa. The total mass of tracer introduced is the same in both cases; however peak initial

concentrations are different due mesh size effects. The primary difference in these simulations is the release location, with D placed on the top of the canisters spreading much more quickly in response to the multiphase thermal convection and heat-pipe/chimney induced by heating. For D placed initially beneath the canisters on the floor of the room, migration is delayed. The ratio of maximum concentration after 10 days to initial concentration for release at the top is 0.018 while for the bottom release this ratio is 0.085. These types of simulations will be vital in design and implementation of tracers tests that can provide data on field scale behavior of the long term heater tests In addition to migration of D and O^{18} in the RoM pile, these tracers will be quite useful in detecting migration of water vapor throughout the test facility, including through the DRZ and possibly around bulkheads to the access drifts.

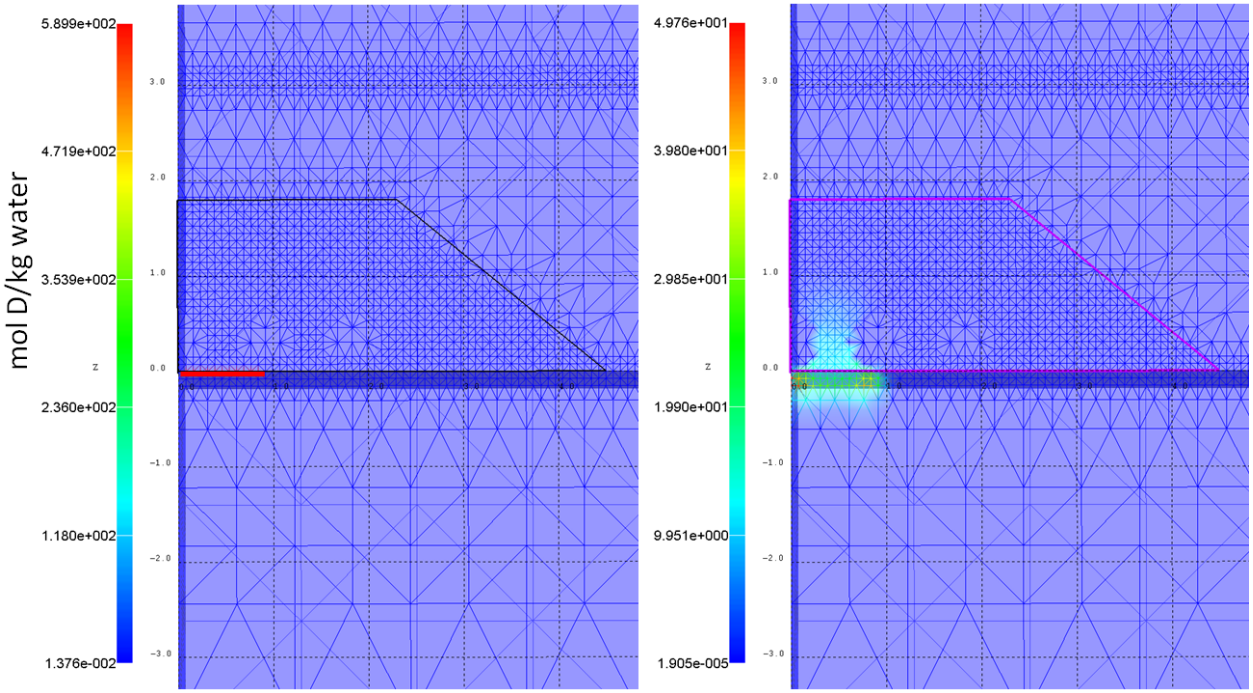

Figure 5.3_2 A) intial spike of deuterium (red line directly beneath the canisters and B) migration and dilution of deuterium after 10 days simulated time.

For a non-spiked case, Figure 5.3_3 shows that the rapid heating of the 750W case leads to measurable fractionation of D away from the initial concentration of 1.73×10^{-2} (mol D/kg liquid water) within 10 days. Regions above the boiling line are depleted due to lighter concentration dropping out of the vapor phase, while around the canisters, boiling is preferentially driving the lighter hydrogen away and leaving a signal enriched in D. Although more vigorous in the high wattage heat pipe examples, our simulations show measurable impacts even in low wattage (250W) cases with no heat-pipe. However, the spiked D or O^{18} signal would be easier to detect as it migrates further from the release location and may be more useful for understanding migration in the DRZ due to barometric pumping and drift ventilation pressure gradients.

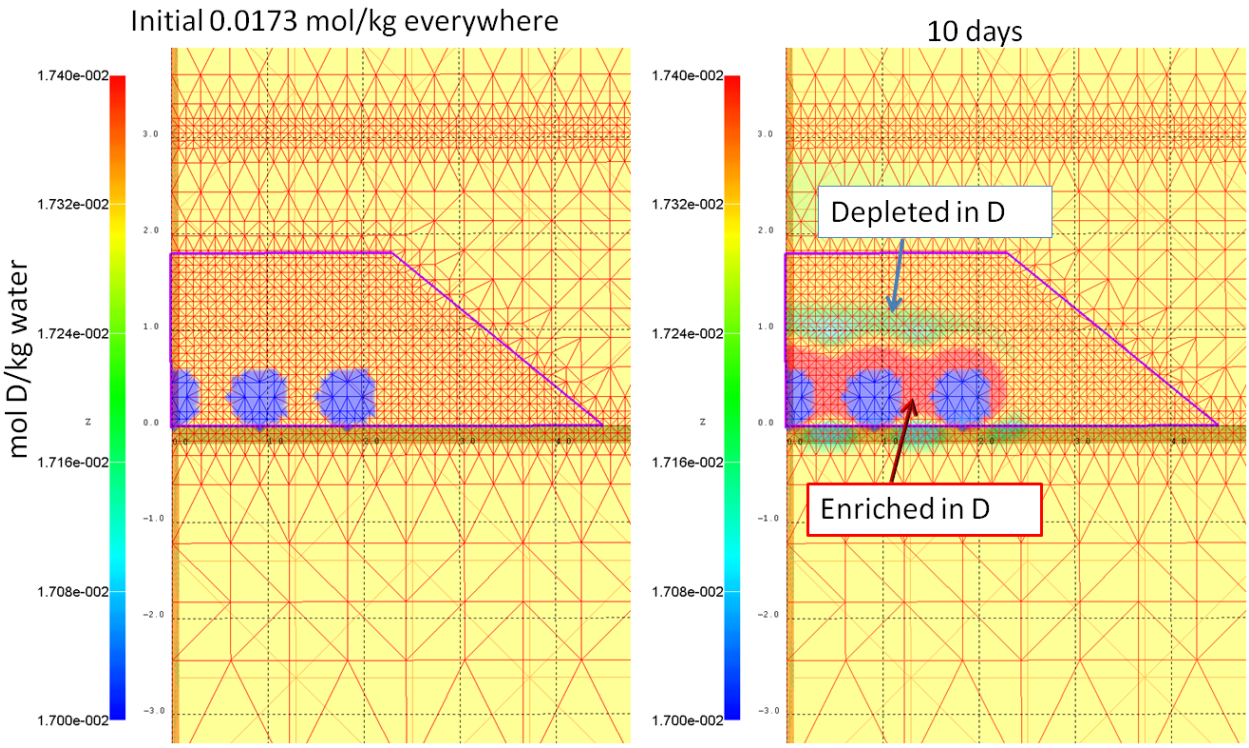

5.4 Evaporation from the Run of Mine (RoM) salt pile

5.4.1 Simple evaporation function

A preliminary function for evaporation has been implemented for RoM salt on the drift-scale simulations. For this effort, we employed a previously developed and benchmarked function for simulating evaporation from a weighing lysimeter at the Nevada Test Site (Stauffer et al., 2008; Scanlon et al., 2005). A relatively simple function was estimated for evaporation as a function of the saturation (sat) at the top of a 1-D column of alluvium:

Evaporation Rate (kg/(s m^2) = 9.e-6*sat + 5.e-5*(sat^2)

This function was created by forcing FEHM to match the lysimeter data and backing out the saturation for each water loss rate at a given time. Results for the function developed for the NTS example are shown in Figure 5.4.1_1 and the fit versus rainfall is shown in Figure 5.4.1_2.

Within FEHM, a special flag is set to call this function for a set of nodes defined in a separate file. For the drift-scale simulations, the evaporation function is applied to top surface of the RoM salt (Figure 5.4.1_3). This same technique could easily be done for RoM salt using a high resolution scale such as pictured in Figure 5.4.1_4 and already being used on the current project. The goal of using the NTS function was to begin looking at evaporation from the top of the pile of salt, and this process can be most easily controlled in the simulations with a simple function. The parameters can be adjusted to allow more or less evaporation to explore a range of possible scenarios which are more difficult to simulate using barometric pumping of variably humid air (Jordan et al., 2014; Neeper and Stauffer 2012a,b; Neeper and Stauffer 2005). Barometric pumping on the scale of the drift-scale simulations will require long simulation times and will be

attempted after more understanding is developed through use of the simpler evaporation function. Figure 5.4.1_5 shows the values of evaporation in the range of RoM studied.

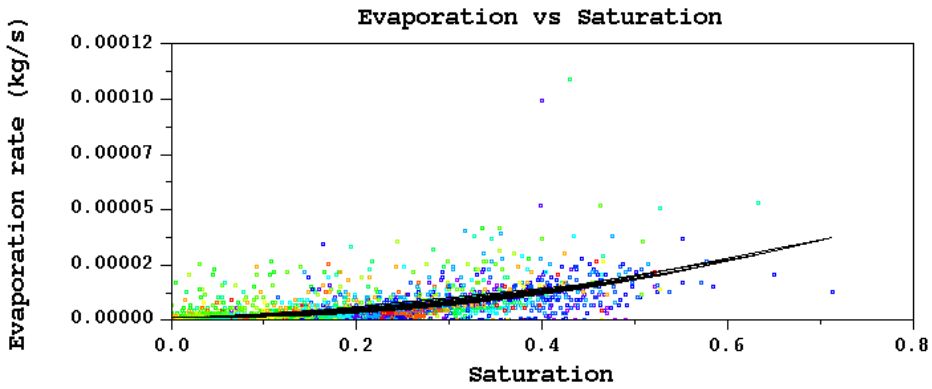

Figure 5.4.1_1 Regression fit to FEHM simulation forced to match lysimeter evaporation.

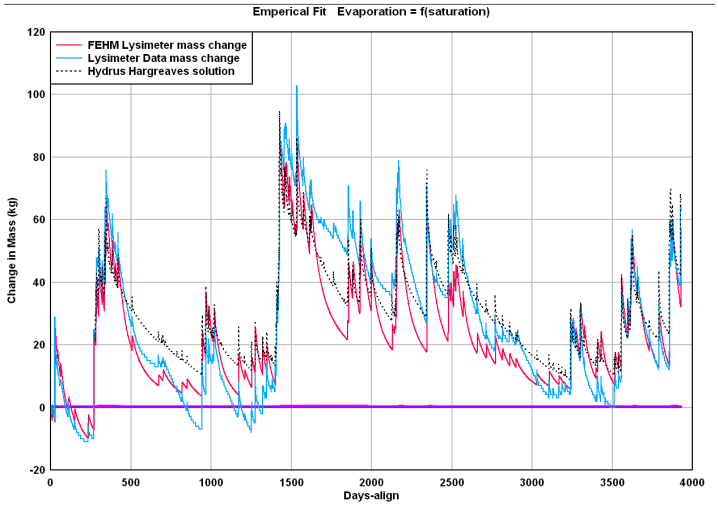

Figure 5.4.1_2 Fit between the FEHM function, lysimeter data, and Hydrus 2D calculations for a 10 year period.

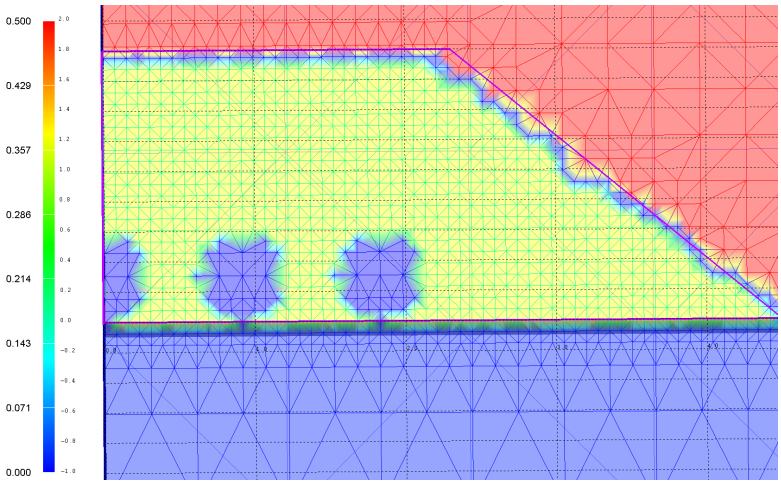

Figure 5.4.1_3 Evaporation nodes at the interface between the RoM salt (yellow) and the drift air (red) are shown as a thin blue line.

Figure 5.4.1_4 Measuring system to determine water loss from a sample in the underground at WIPP (Photo from Sean Otto).

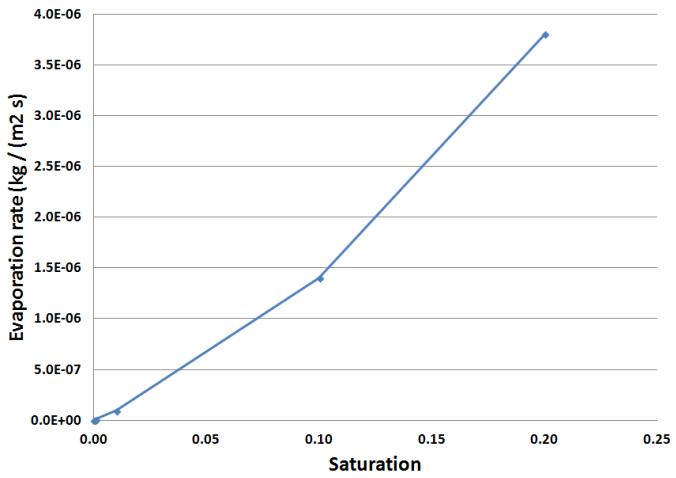

Figure 5.4.1_5 Evaporation versus saturation function in the range of RoM salt.

5.4.2 Drift-scale evaporation simulation results

Figure 5.4.2_1 shows the impact of evaporation on the RoM salt saturation. The high evaporation caused by the NTS function leads to 200 kg of water loss from the pile relative to a pile with limited evaporation. This is extremely significant in that such water loss could reduce the formation of a heat-pipe in the RoM salt. However, preliminary results from an evaporation experiment in the underground at the WIPP facility (Figure 5.4.2_2) show much lower evaporation from a beaker of RoM salt than was measured at the NTS lysimeter. In this preliminary data, virtually no net change in mass was recorded during first half of the experiment while the relative humidity in the facility was above 15%. Only when relative humidity dropped

below 15% was a noticeable trend in evaporation from the RoM salt seen. To address this complexity, lower evaporation functions will created by fitting more extensive data (yet to be gathered) in a manner similar to the work described for the NTS lysimeter.

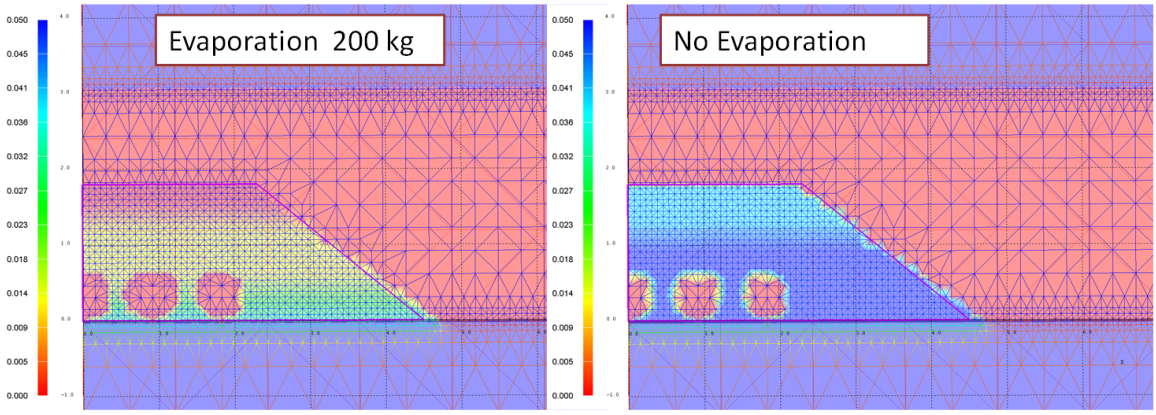

Figure 5.4.2_1 60 days of 750W heating with 1.25% water content for A) evaporation function and B) no evaporation function.

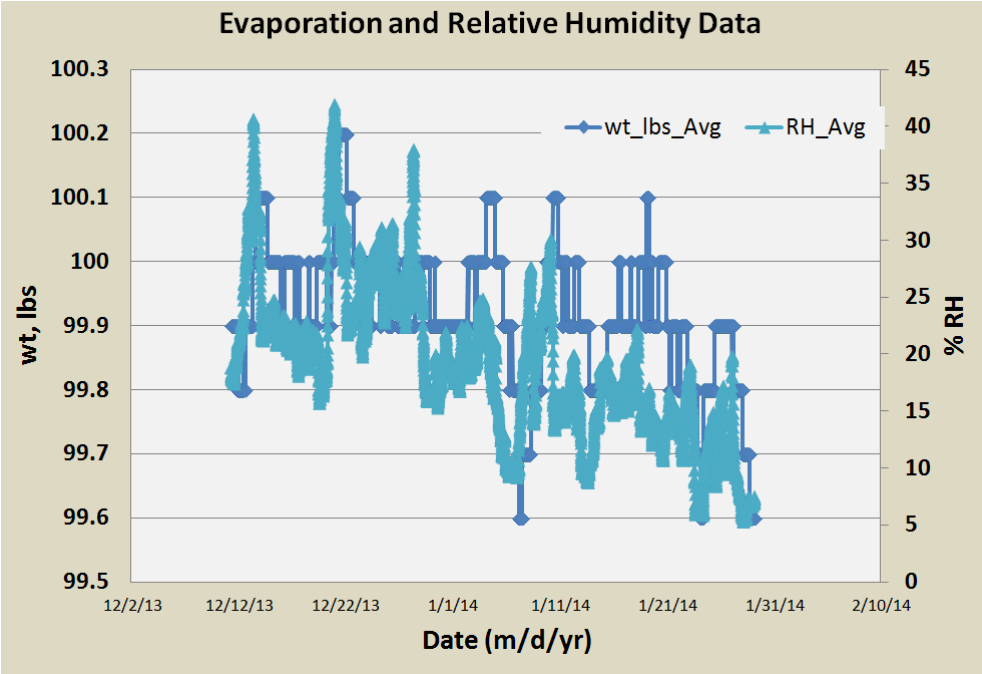

Figure 5.4.2_2 Preliminary data from a beaker of RoM salt that was located in the WIPP facility near the proposed large scale heater test.

5.5 New drift-scale computational mesh

A new computational mesh was created in Nov 2013 after the project decided to increase the depth of burial on the hypothetical waste canisters to 8 ft. (2.42 m). The new mesh is shown in Figure 5.5_1 and is a ¼ space using the two reflection boundaries along the horizontal center of

the hypothetical waste cylinders. The cylinders pictured would be 10 ft long with a 2 ft radius in full 3-D, however in quarter symmetry as shown, the middle most cylinder (blue) is 5 ft long by 1 ft wide (1/4 of a cylinder) and the other two shown in cross section are 5 ft long by 2 ft wide. The full domain simulates 5 waste canisters lying approximately 1 ft apart. These details are the same as in the mesh used for Stauffer et al. (2013). The additional height of the RoM salt leads to a final difference; due to using a constant angle of repose of the RoM salt and a fixed lateral extent of the salt pile, the length of the horizontal top of the salt pile is shorter in the new mesh.

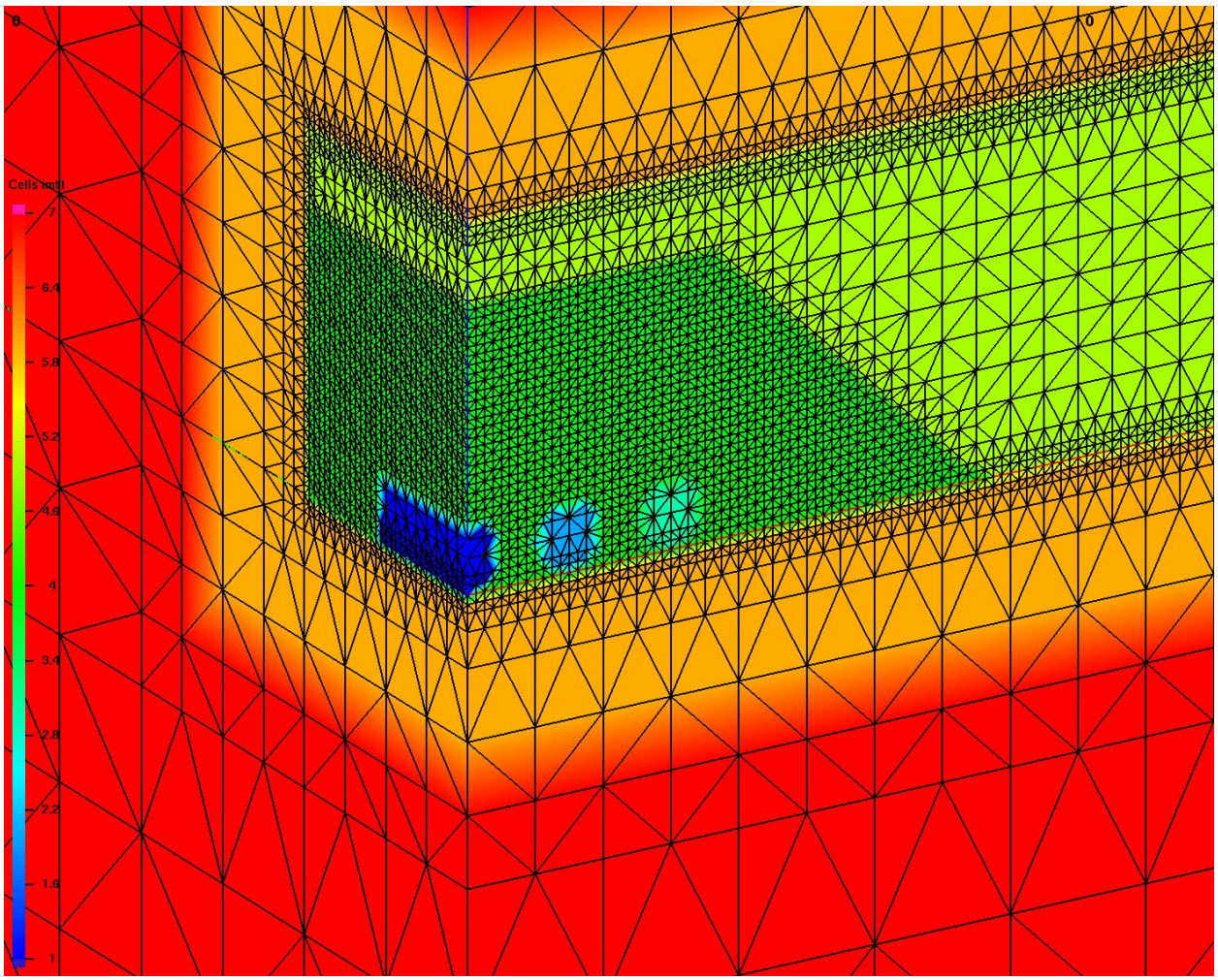

5.5_1 New computational mesh with 2.4 m (8ft) RoM salt pile.

6. References

Cinar, Y., G. Pusch, and V. Reitenbach, 2006. Petrophysical and Capillary Properties of Compacted Salt, Transport in Porous Media, 64, 199-228.

Jordan, A.B., P.H. Stauffer, D. Reed, H. Boukhalfa, F.A. Caporuscio, B.A. Robinson (2014) Draft Test Plan for Brine Migration Experimental Studies in Run-of-Mine Salt Backfill, Los Alamos National Laboratory Document LA-UR-14-27338.

Jordan, A.B., P.H. Stauffer, G.A. Zyvoloski, M.A. Person, J.K. MacCarthy, and D.N. Anderson (2014). Uncertainty in Prediction of Radionuclide Gas Migration from Underground Nuclear Explosions., Vadose Zone Journal, First Look, doi:10.2136/vzj2014.06.0070.

Kreith, F, and M.S. Bohn, 1993. Principles of Heat Transfer, 5th ed., St. Paul, MN: West Publishing Company, p. 176.

Kuhlman, K.L. and Malama, B. (2013). *Brine Flow in Heated Geologic Salt*. SAND2013–1944, Albuquerque, NM: Sandia National Laboratories.

Kwicklis, E.M., A.V. Wolfsberg, P.H. Stauffer, M.A. Walvroord, and M.J. Sully (2006), Multiphase Multicomponent Parameter Estimation for Liquid and Vapor Fluxes in Deep Arid Systems Using Hydrologic Data and Natural Environmental Traces, *Vadose Zone Journal*, 2006 5:934-950

Olivella, S., S. Castagna, E. E. Alonso, and A. Lloret, 2011. Porosity variations in saline media induced by temperature gradients: experimental evidences and modeling. *Transport in porous media* 90, no. 3, p763-777.

Neeper, DA; and Stauffer, P (2012a), Transport by Oscillatory flow in Soils with Rate-limited Mass Transfer I. Theory, *Vadose Zone J* , doi:10.2136/vzj2011.0093.

Neeper, DA; and Stauffer, P (2012b), Transport by Oscillatory flow in Soils with Rate-limited Mass Transfer II. Field Experiment, *Vadose Zone J* , doi:10.2136/vzj2011.0094.

Neeper, DA; and Stauffer, P (2005), Unidirectional gas flow in soil porosity resulting from barometric pressure cycles, *Journal of Contaminant Hydrology*; v.78, no.4, p.281-289

Robinson, B. A.; Elkins, N. Z.; Carter, J. T., Development of a U.S. nuclear waste repository research program in salt. *Nuclear Technology* 2012, *180*, 122-138.

Scanlon, B. R., D. G. Levitt, et al. (2005). Ecological controls on water-cycle response to climate variability in deserts. Proc. Natl. Acad. Sci. 102(17): 6033-6038.

Stauffer P.H., Robinson, Nelson, Harp, Jordan, Boikhalfa, Laybed, Ten Cate (2014), Simulations in Support of the Salt Defense Disposal Initiative (SDDI): Water and Salt Transport Driven by Heat Generating Nuclear Waste in Bedded Salt, WM-14, LA-UR-13-27584.

Stauffer, P.H., D.R. Harp, A.B. Jordan, Z. Lu, S. Kelkar, Q. Kang, J. Ten Cate, H. Boukhalfa, Y. Labyed, P.W. Reimus, F.A. Caporuscio, T.A. Miller, and B.A. Robinson. (2013).

Coupled model for heat and water transport in a high level waste repository in salt. Los Alamos National Laboratory Document LA-UR-13-27584. (2013)

Stauffer, P.H., E.M. Kwicklis, M.J. Sully (2008), Modeling evaporation from a non-vegetated lysimeter experiment, LA-UR-08-0481).

Stauffer, P.H.(2002), Tritium transport beneath surface impoundments at TA-53 modeling and analysis in support of data needs, Los Alamos National Laboratory Report, LA-UR-02-5321.

Stauffer P.H., and Rosenberg, N.D. (2000), Vapor phase transport at a hillside landfill, *Environmental and Engineering Geoscience*, Vol. VI, No. 1, p. 71-84

Stauffer P.H., Auer, L.H., and Rosenberg, N.D.(1997), Compressible gas in porous media: A finite amplitude analysis of natural convection, *Int. J. of Heat and Mass Transfer,* 40 (7), 1585-1589.

Zyvoloski, G.A., B.A. Robinson, Z.V. Dash, and L.L. Trease. 1997. Summary of the models and methods for the FEHM application— A finite-element heat-and mass-transfer code. Rep. LA-13307-MS. Los Alamos National Laboratory, Los Alamos, NM. .

7. Appendix I : Draft Journal Article

Clay Dehydration around Heat-Generating Nuclear Waste in Bedded Salt Formations

Amy Jordan, H.F. Boukhalfa, F. Caporuscio, B.A. Robinson, P.H. Stauffer

Abstract

Disposal of high-level nuclear waste (HLW) in bedded salt is modeled using the Finite Element Heat and Mass transfer code (FEHM), which simulates highly coupled thermal, hydrological, and chemical processes in porous material. Within the temperature range that can be reached by canisters of waste in the HLW inventory, drift-scale modeling shows that a heat pipe may be established in salt with strong feedbacks on the final temperature, moisture, and mechanical state of the system. Because the extent of heat pipe activity depends on the amount and mobility of water in the salt surrounding the waste, a model is needed for water release from clay dehydration as a function of temperature. Run-of-mine (RoM) impure salt samples from the Waste Isolation Pilot Plant (WIPP) were heated to specific temperatures and the mass of water released was measured. These data were used to develop a source term for moisture in the FEHM code. Simulation results are presented for over a year of heating by 750 W waste canisters in a waste drift in bedded salt with RoM backfill, assuming varying clay fractions from 0–10% by mass. In some cases, clay dehydration provides sufficient moisture to sustain a heat pipe where models neglecting this process do not.

Introduction

The question of where to store the nation's high-level nuclear waste (HLW) provides motivation for scientific research on the safety of geologic disposal options. A number of potential geologic media have been proposed for HLW repositories, including shale, clay, low-permeability crystalline basement rocks, volcanic tuff deposits within the vadose zone, and bedded salt.

There are multiple geologically stable salt formations in the U.S. that may be suitable for nuclear waste disposal, and salt has unique temperature-dependent viscoplastic properties that contribute to self-sealing and extremely low permeabilities; it has a high thermal conductivity; and it is easy to mine (Hansen and Leigh, 2012). All of these characteristics are favorable for the siting of a nuclear waste repository. To understand the long-term performance of a salt repository, it is important to quantify fluid transport during the first few years of heated waste emplacement. A prediction of the moisture state immediately surrounding the canisters is critical for performance assessment models because corrosion and breakdown of the waste by microbial activity could occur if the conditions are conducive to it (Davies, 1991). Local saturation also affects the salt plasticity and mechanical deformation that take place after emplacement of heated waste.

One concept for disposal of HLW in bedded salt that builds on knowledge gained at the Carlsbad, New Mexico Waste Isolation Pilot Plant (WIPP) repository for transuranic (TRU) nuclear waste is known as the "in-drift" waste emplacement strategy (Carter et al., 2012). In this method, which was not used at WIPP, waste drifts are excavated in the bedded salt formation, and the run-of-mine (RoM) excavated material is used as backfill over the waste canisters (Figure 1). Impurities in the bedded salt will be incorporated in the RoM backfill around the waste.

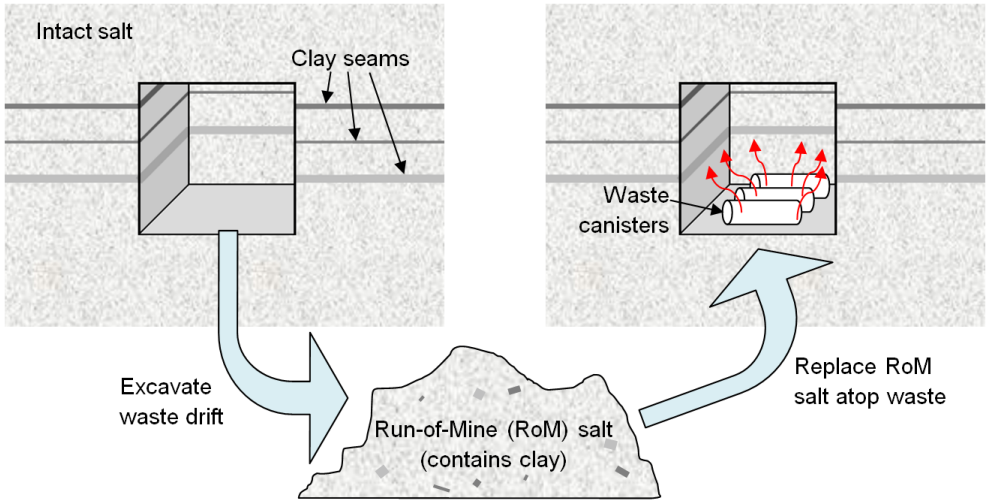

Figure 1. Schematic of the in-drift waste disposal concept.

Depending on the heat load of the canisters, temperatures in the RoM backfill salt may exceed the boiling point of brine. Intact salt is impermeable (around 10^{-22} – 10^{-21} m^2) (Beauheim and Roberts, 2002), but porosity and permeability in the crushed RoM salt will initially be much higher. Assuming there is sufficient available water, these conditions are conducive to heat pipe formation, whereby free water is vaporized in the boiling region, convects and diffuses along concentration gradients to the cooler regions where it recondenses, and replenishment of fluid towards the heat source is established from gravity flow, capillary pressure gradients, and fluid inclusion migration. Where brine re-enters the boiling region, it deposits its salt as a precipitate and contributes to the build-up of a low-porosity rind around the waste.

Evidence of heat pipe formation has been seen in heater tests reaching 130°C at WIPP (Brady et al., 2013; Stauffer et al., 2013), where the low-porosity rind of salt was observed. In other salt repository scenarios where HLW may be emplaced, heat pipe formation could contribute to significant differences in the final temperature, moisture content, and porosity of the backfilled RoM salt around the waste. These changes may be positive, negative, or neutral in terms of performance characteristics of the repository, but their long-term impact can only be quantified if the short-term model accurately predicts the effects.

Numerical simulations of high-temperature waste have been performed by multiple groups for WIPP and for other salt repositories worldwide, particularly in Germany, where bedded salt and salt domes are possible candidates for HLW disposal (Kuhlman and Malama, 2013). These models have been constrained by code limitations to handle specific processes with limited coupling between active thermal, hydrological, mechanical, and chemical (THMC) processes. For example, simulations have been presented with thermal processes sequentially coupled to mechanical (e.g., Clayton and Gable, 2009) and fully coupled TM models have also been developed for salt repository applications (e.g., Stone et al., 2010). A sequentially coupled TH to M model is under development and has been used to model the in-drift waste emplacement concept (Blanco Martin et al., 2013).

Initial coupled THC simulations using the Finite Element Heat and Mass transfer code (FEHM) indicated that the amount of water available in the RoM backfill would play an important role in governing whether an active heat pipe would form or not (Stauffer et al., 2013). Moisture content in salt was determined to be a primary factor affecting the development of the heat pipe, making it one of the governing parameters that drives the uncertainty of the simulations. It is therefore critical to accurately determine the moisture content in salt and its evolution in the heated RoM backfill. Moisture in salt is either associated with the salt itself in the form of finely dispersed inclusion present inside the salt crystals (intera-crystalline), within the grain boundaries between salt grains, or associated to clay and other accessory minerals present

in salt. The mobility of these different populations of water, their chemical composition and their relative amounts vary significantly within the salt bed. Among these different water populations, water associated with accessory minerals in salt (e.g., clay, gypsum) represents the largest fraction of moisture contained in salt. Effectively, clay impurities in salt can represent up to 20 wt. % of the salt, and can accumulate up to 10 wt.% of their weight in water (Caporuscio et al., 2013). Hydration and dehydration properties of clay as a function of temperature become critical to the availability of moisture in salt and the potential development of a heat pipe. Other moisture sources (brine inclusions, moisture adsorbed on salt) are likely less than 0.5 wt.% and might play a lesser role in defining the performance of the salt material. Moisture drawn from the repository floor below the waste is another source of water.

The temperature, timing, and amount of water released from clay layers and accessory minerals depends sensitively on the presence of electrolytes, relative humidity, in-situ temperature, and pressure (Caporuscio et al., 2013). Limited relevant experimental data exist on the water-releasing phase transitions in clays and other accessory minerals in bedded salt formations. Bound interlayer water in corrensite, a primary clay identified at WIPP, can be released above 75°C:
$(Ca, Na, K)(Mg, Fe, Al)_9(Si, Al)_8O_{20}(OH)_{10}\cdot 9H_2O = (Ca, Na, K)(Mg, Fe, Al)_9(Si, Al)_8O_{20}(OH)_{10} + 9H_2O$

Following loss of interlayer water, corrensite is stable to temperatures above 275°C (Caporuscio et al., 2013).

A number of previous studies examined the changes in smectite clay at elevated temperatures and/or pressures. Altaner and Ylagan (1997) provide a good introduction to the concepts of smectite alteration. Smectite illitization is considered to proceed through mixed-layer illite/smectite (I/S) intermediates as the percentage of illite interlayer increases. Important factors for the changes include increasing temperature, potassium (K) concentration, time, and water/rock ratio. Possible reaction mechanisms for smectite illitization include solid-state transformation, dissolution and crystallization, and Ostwald ripening. Wu and colleagues (Wu et al. 1997) examined partially dehydrated Ca- and Mg-exchanged montmorillonite by heating samples at pressures from the H_2O liquid-vapor boundary to about 10 kbar. Progressive dehydration caused shrinkage of the crystal lattice from the 19 Å hydration state to the 15 Å at 260-350 ºC with further dehydration to the 12.5 Å state at higher temperature. Mg-montmorillonite dehydrates to the 15 Å state at 200-250 ºC, with further dehydration to the 12.5 Å state at 590-605 ºC. Similar experiments with Na-exchanged montmorillonite (Huang, 1994) identified shrinkage from the 19 Å hydration state to the 15 Å hydration state at 330-385 ºC and from 15 Å to 12.5 Å at 485-500 ºC. The 19 Å fully hydrated montmorillonite, therefore, is stable up to 200-380 ºC under pressure in the absence of potassium.

Ferrage et al. (2011) presented some of the best evidence for the mechanism of S to I/S transformation. They studied the hydrothermal reactivity of K-exchanged low-charge montmorillonite (SWy-2) at 250-400 °C and 1 kbar, with reaction times of 5 to 120 days. The authors provided experimental evidence for a dissolution-crystallization mechanism following the Ostwald step rule in which metastable smectite transforms into illite through a series of metastable illite-smectite phases. Dehydration and lattice shrinkage that occurs in this temperature range is fully or almost fully reversible. However, at higher pressures, the rehydration initially follows a lower-temperature path relative to the thermal path of dehydration.

The effect of dehydration was examined at 250, 500, and 650°C by treating samples for 1 hour at designated temperatures (Krumhansl, 1990). Their results show significant structural alterations as a result of the heat treatment. The peaks characterizing the chlorite and corrensite are significantly reduced by the heating process. However, the illite peak remains prominent throughout the various heat treatments examined (Krumhansl, 1990).

Sulfate minerals are also identified in WIPP samples, such as gypsum, anhydrite, and polyhalite. Gypsum ($CaSO_4 \cdot 2H_2O$) can transition directly to anhydrite ($CaSO_4$) or to metastable bassanite ($CaSO_4 \cdot 0.5H_2O$), followed by a bassanite to anhydrite transition at hotter temperatures. Temperatures for these transitions have been measured for several scenarios by previous authors, and range from 25°C – 52°C for direct gypsum to anhydrite (Freyer and Voight, 2003); 76°C for gypsum to bassanite (Freyer, 2000); and greater than 140°C for bassanite to anhydrite (Shcherban and Shirokikh, 1971). These transitions can release up to 21% weight loss as water. Polyhalite, $K_2Ca_2Mg(SO_4)_4 \cdot 2H_2O$, loses its hydrate water at temperatures above 250°C (Caporuscio et al., 2013), and can lose 6 wt% as water. Other minerals that may be present include carnallite ($KMgCl_3 \cdot 6H_2O$), which can lose 38 wt% as water; kieserite ($MgSO_4 \cdot H_2O$); and bischofite ($MgCl_2 \cdot 6H_2O$) (Caporuscio et al., 2013).

New dehydration results are presented for heated WIPP samples from representative RoM salt, as well as clay-rich and relatively pure halite samples. These results are used to create a model of clay dehydration in bedded salt which is implemented in a numerical simulator for coupled thermal, hydrological, and chemical processes in a HLW in-drift disposal scenario.

Experiments

Salt sampling and characterization

Run-of-mine-salt obtained from current excavations at WIPP was obtained in a sealed container to preserve its moisture content. The samples were processed manually by sieving through different sieve sizes to determine their size distribution and used for moisture release experiment. Blocks larger than 10 cm were removed before sieving and weighed separately.

Characterization of accessory minerals associated with salt

Gravimetric characterization of salt dehydration

Thirteen samples (100 to 200 g) were collected from WIPP that represented a range of impurity content and mass fractions in the salt, including mapped units such as clay seam F, the orange marker bed, crushed RoM salt, and relatively pure halite from the drift floor in a freshly excavated room (Caporuscio et al., 2013). Residual minerals from the samples were analyzed by X-ray diffraction. Residues from clay seam F and orange marker bed samples were composed primarily of corrensite with minor amounts of quartz, magnesite, mica, kaolinite (or possibly chlorite), hematite, and anhydrite. All samples contained halite.

The samples were weighed, heated at the designated temperature, and weighed again every 8–12 hours until the weight stabilized (typically, within 24–72 hours). Once a constant weight was achieved at the first temperature, the sample was heated to the next desired temperature and the process was repeated. The temperatures were 65°C, 110°C, 165°C, and 265°C. A portion of the samples were removed from the heaters after 65°C and 110°C and allowed to rehydrate to test the reversibility of the water loss.

We examined water content in salt rock samples collected from WIPP. The samples examined in this study were collected from the clay seam F, and the orange marker bed, and pure halite beds[ref, Figure ?]. The samples were sealed in plastic bags using an impulse heater immediately after exiting the underground mine, and were kept in sealed large plastic container until utilized. Total water content and water release as a function of temperate were determined gravimetrically by heating thirteen discrete samples of about 100 to 200 grams each to different temperatures and recording the weight loss at each temperature. The samples were minimally desegregated by hand and the weight of each sample was

recorded at the start of the experiment and every 8 to 12 hours during the dehydration experiment. The samples were left to dehydrate at each designated temperature until the weight of the samples was constant (typically 24 to 72 hours). The dehydration experiments were performed in a heating oven equipped with exhaust vales that allow the control of the oven vacuum. The samples were gradually heated to 65 ^{o}C, 110 ^{o}C and 265 ^{o}C respectively. The maximum vacuum applied was 15 mmHg at 265 ^{o}C to ensure the release of all water associated with the rock salt. The moisture released from these experiments was not collected. In a separate experiment, we connected the heating oven to a vacuum trap cooled with crushed ice to collect the water released from the salt. Although some water was collected in the trap, its mass was significantly less than the weight loss recorded for the salt. This is to be expected because of the water loss due to the strong vacuum applied.

Thermogravimetric analysis (TGA) of salt and accessory minerals

Results and Discussion

Moisture release from run of mine salt as a function of temperature

Figure 2 shows weight loss of the samples with time and heating. An initial weight gain ranging from 0.1–0.8 wt% occurs for all samples, which was due to moisture absorption during equilibration of samples at room temperature before the start of the dehydration experiment. Heating clay-rich samples to 65^{o}C resulted in total sample weight loss of 1.2–2.1 wt%, with clay-rich samples losing the most water. By fraction of clay and other accessory minerals (abbreviated as "clay mass" from here, but potentially including water loss from polyhalite, gypsum, and other hydrous minerals), the water loss was 12.1–19.6% of clay mass (average 14.8%) at 65^{o}C. The clear salt samples lost less than 0.25 wt% of their total weight at 65^{o}C. The dehydration of the clay rich samples at 65^{o}C was reversible; 3 samples removed from the oven and placed in a moist chamber recovered their weight and then continued to accumulate water rapidly.

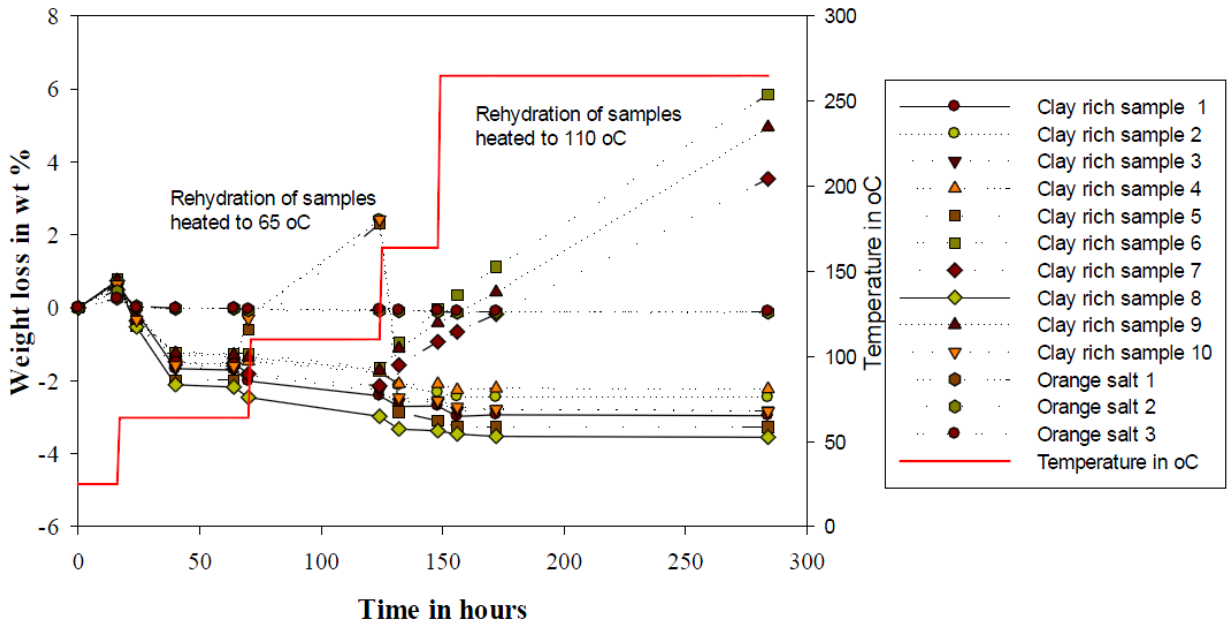

Figure 2. Sample weight loss as a function of time for 13 salt samples of varying accessory mineral content. Rehydration of 3 samples heated to 65^{o}C shows the weight gain from a humid environment at room temperature. Similarly, rehydration occurred when samples heated to 110^{o}C were removed from heat and placed in a humid environment at room temperature.

The clay-rich samples heated to 110°C lost 1.3–2.5 wt%. By clay fraction this was 14.6–20.4% of clay mass, with an average of 17.3% (or 2.5% additional mass loss from dehydration following the water loss at 65°C). For clear salt with minimal accessory minerals, water loss was less than 0.06 wt%.

At 165°C, the samples lost no additional weight after heating for approximately 15 hours. The dehydration process was reversible for all samples heated to 165°C and then removed to a moist environment (Figure 2). These samples rapidly recovered all the moisture lost and then accumulated moisture far beyond their original moisture content, indicating that (a) the transformations observed are reversible and (b) that clay is the dominant accessory mineral associated with salt, as it can undergo reversible hydration/dehydration processes.

The temperature was raised to 265°C for the final test of water loss. Samples lost total 0.09–3.5 wt %, or 20.1–28.7% of clay mass (average of 24.0%, or 6.7% more water lost by clay following the previous dehydration to 110°C).

The amount of moisture released by the samples is correlated with their accessory mineral content (Figure 3), rejecting the hypothesis that the water released is primarily intergranular pore fluid or intragranular brine inclusions for the clay-rich samples. Furthermore, the reversible water loss for T < 110°C is consistent with temperatures under which corrensite undergoes hydration/dehydration processes: the XRD results provide strong evidence of loss of interlayer water (5–13 wt%) at 65–75°C (Caporuscio et al., 2013). Concurrently, at around 75°C, the gypsum to bassanite phase transformation can release up to 21 wt% water (Caporuscio et al., 2013). The low-temperature water loss (<65°C) may be from evaporation of mobile pore fluid or the beginning of the gypsum transitions. The cause of the water loss at higher temperatures may be from further dehydration of both mineral groups, particularly bassanite to anhydrite, but additional experimental work is necessary to confirm the nature of these high-temperature dehydration processes.

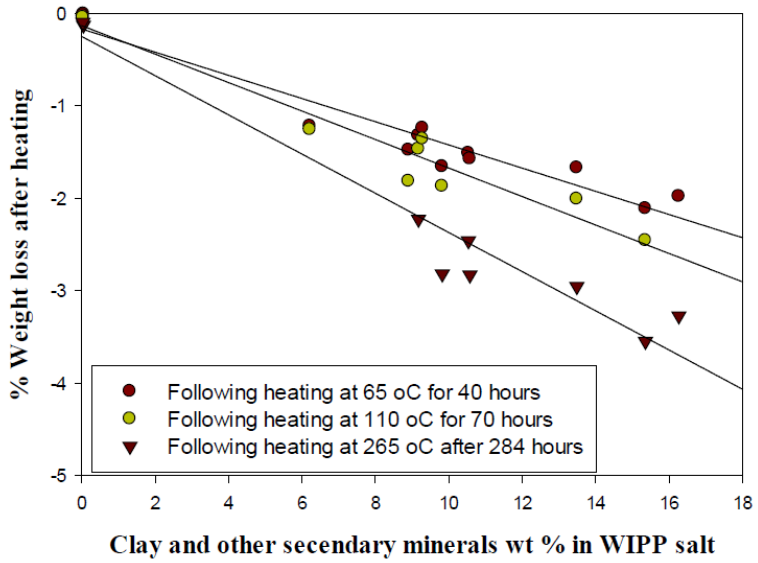

Figure 3. Weight loss as a function of temperature and heating duration for salt samples collected from WIPP. Samples with high secondary mineral content were collected from clay seam F and the samples with low secondary mineral content were from the orange marker bed.

Numerical Model

Methods

We implemented a basic clay dehydration model based on the experimental results above into FEHM, a

multiphase flow and transport model developed at Los Alamos National Laboratory (LANL) (Zyvoloski et al., 1997). FEHM uses the control volume finite element method to find approximate solutions to the governing equations of mass and momentum conservation, assuming a multiphase form of Darcy's Law is valid for all phases across the domain. Many new capabilities have been added to FEHM to enable the tightly coupled THC processes of fluid transport in heated salt (Stauffer et al., 2013), including: porosity change from the precipitation/dissolution of salt, with salt solubility as a function of temperature; permeability as a function of variable porosity; thermal conductivity of salt as a function of porosity and temperature; vapor pressure of water as a function of concentration and temperature; water vapor diffusion coefficient as a function of saturation, porosity, pressure, and temperature; and more. Simulations have been tested against recent and historical experimental data to develop and improve the salt material model (Stauffer et al., 2013; Caporuscio et al., 2013).

Averages of the water loss data as a function of temperature were used in the clay dehydration model implemented in FEHM (Figure 4). The model uses a simple stair-step function, and does not allow rehydration. Because the temperatures remain elevated in the backfill salt around the waste for the duration of the model runs, rehydration is not expected.

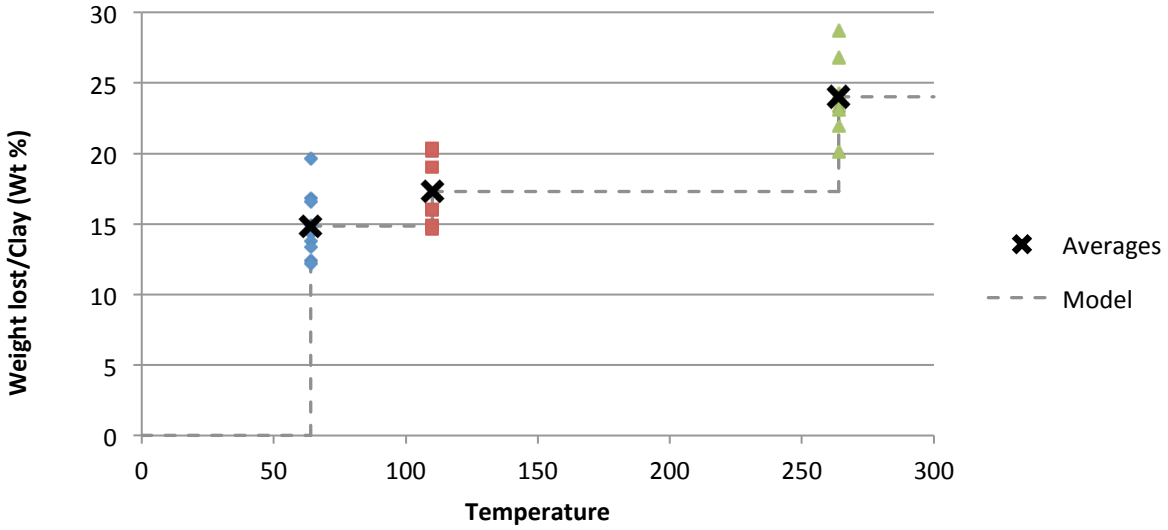

Figure 4. Weight lost as a percentage of clay weight during the heating experiment. The clay dehydration model is a stepwise function that produces the appropriate mass of water release when the model reaches the temperatures indicated (65, 110, and 265°C).

As implemented in FEHM, the clay dehydration model can be applied to selected nodes or zones within the model, and differing clay fractions can be specified across the model. Based on the averaged experimental data, at 65°C, 14.8% of the mass of clay in the node is added as a source term in a one-time release. At 110°C, an additional 2.5% of the clay mass is released, and at 265°C, an additional 6.7% is released. For a given node for which the clay dehydration model is invoked, for a specified clay mass fraction f_c, the mass of water produced for the first 65°C dehydration is given by

$$M_w = 0.148\, f_c\, (1 - f_i)\, \rho_c\, V_{cell} \qquad (1)$$

where f_i is the initial porosity of the node, ρ_c is the density of clay, and V_{cell} is the volume of the node. The water mass production for the second and third clay dehydration temperatures follows similarly.

The implementation of dehydration in FEHM was tested by running a 6-node model of composed of crushed salt with many of the same relevant physical processes as the full model (Stauffer et al., 2013). Total water production for the 6-node problem was correct to within 2% of the expected amount for all cases tested, with many cases correct to within 0.5%.

The clay dehydration model was used in numerical simulations of a drift in a HLW repository. Five heated waste cylinders, 1 m in radius, were spaced 0.3 m apart on the floor of a 4.9 m wide by 3.0 m high (16 ft wide by 10 ft high) drift. Salt backfill over the canisters extended 1.8 m (6 ft) in height above drift floor. A section of the numerical mesh developed for simulations of this experiment is shown in Figure 5. The model represents a quarter of the space, with reflection boundaries on both faces seen in Figure 5. The zones represent the undisturbed, intact salt of the repository; the damaged rock zone (DRZ) with enhanced permeability due to damage related to excavating the drift; air; the RoM salt backfill; and the metal heaters. Clay seams are not modeled in the drift walls, but the RoM backfill was modeled to contain 0–10% clay by weight.

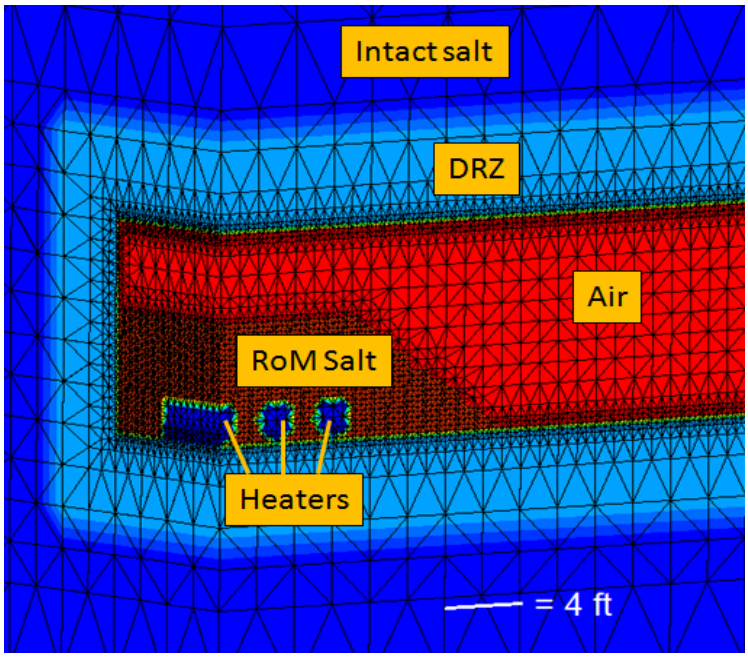

Figure 5. Numerical mesh showing the zones of the model: intact salt, damaged rock zone (DRZ), air, run-of-mine (RoM) backfill, and the heated waste canisters. Reflection boundaries along the left and front faces shown in this image complete the 3-D space with 5 canisters.

Initial saturation for various model runs was 1–10% in the crushed salt. Maximum capillary suction at residual saturation ranged from 0.2–1 MPa. The heat load was 750 W per canister, a mid-range temperature canister for the defense HLW inventory.

Results

For a case with 1% initial saturation in the RoM salt and 0.2 MPa maximum capillary suction, temperature and saturation for three RoM salt nodes above the center canister versus time are shown in Figure 6. The closest node to the heater (z = 0.61 m) reaches 65°C and releases water at 2.2 days. This node reaches 110°C at 8.8 days and more water is released, but the released water goes directly to the vapor phase and there is a dip in temperature as the water produced is boiled. The next nearest node to the heater (z = 0.99 m) reaches 65°C at 7.8 days and 110°C at 90 days. The furthest node from the heater at the top of the RoM pile (z = 1.6 m) does not reach 65°C and thus releases no water. The simulation was run for a total length of 460 days.

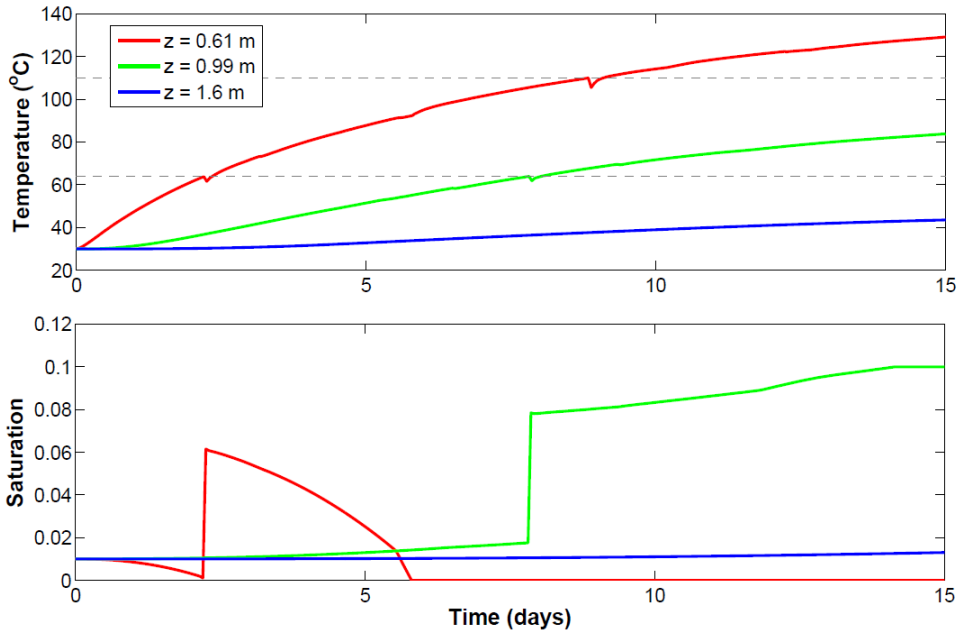

Figure 6: Temperature and saturation for three nodes with increasing distance from the central heater in the simulation with 10% clay in the RoM salt, initial saturation of 1%, and 0.2 MPa maximum suction.

Temperature, saturation, and porosity at 460 days are shown in Figure 7. Although initial saturation was 0.01, clay dehydration produces additional water, which migrates outside the boiling region. There is little change in porosity from the initial state, which is zero porosity in the heaters (blue circles in Figure 7c) and 35% in the RoM salt (yellow in Figure 7c). There is an increase in porosity in small gaps between the heaters from early-time (pre-boiling) dissolution of salt as brine flux from the EDZ increases in temperature and dissolves more salt. Additionally, a slight changes in porosity are seen from the initial 35% within the salt pile. However, there is no real, sustained heat pipe in this case, which would lead to porosity reduction around the heaters.

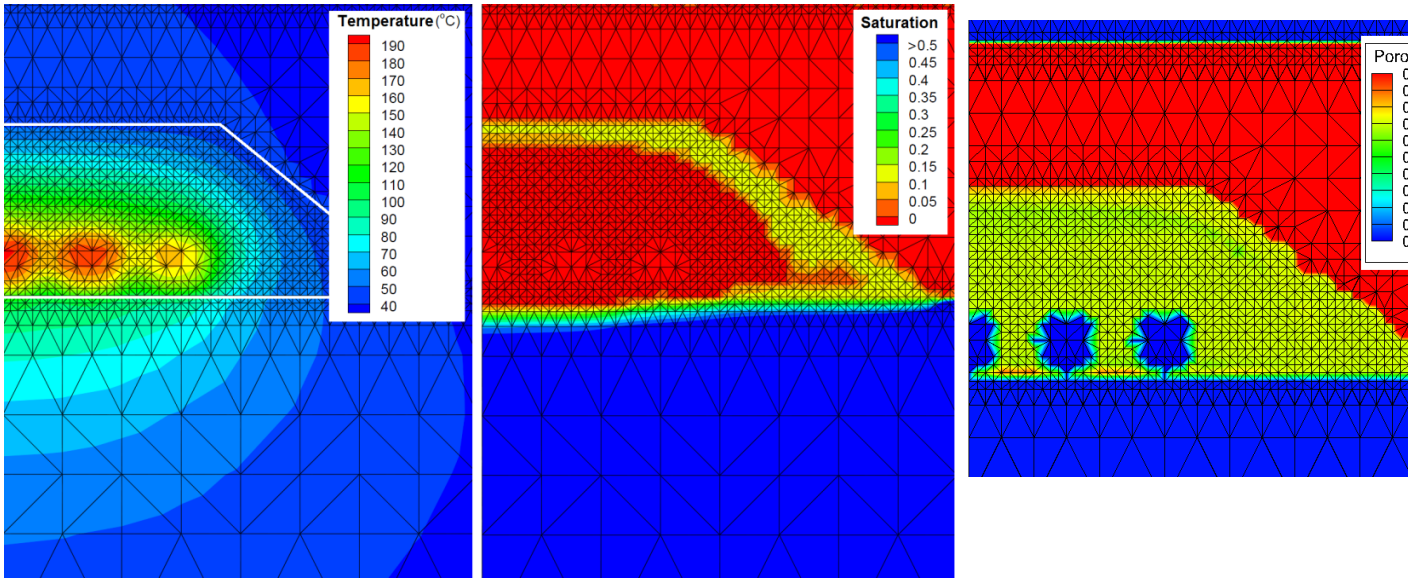

Figure 7: (a) Temperature, (b) saturation, and (c) porosity at 460 days around the heaters.

The total amount of water produced by clay in the RoM salt pile in the model (one-quarter of the full salt pile) is 119 kg at 460 days. By comparison, the total initial amount of water in the RoM salt with initial saturation of 0.01 and porosity 0.35 is 50.4 kg. That is, the clay dehydration produces a significant amount of water, but there is still not enough available or mobile moisture to sustain a heat pipe.

On the other hand, the same properties at 460 days are shown in Figure 8 for a case with initial saturation of 0.07 in the crushed salt, 1 MPa maximum capillary suction at zero saturation, and – as above – 10% clay. In this case, there is clear evidence of a sustained heat pipe, with significant porosity reduction around the heaters and an extreme porosity increase at the condensation arc. (In reality, a salt pile *may* reconsolidate to compress the hollowed-out arc, or it may support the cavern, depending on complex mechanical factors that we do not model.)

While the case with clay dehydration shown in Figure 8 produces an obvious heat pipe, the corresponding case with no clay dehydration does not product a heat pipe. Saturation, porosity, and temperature differences at 460 days between 10% clay and the corresponding simulation with no clay are shown in Figure 9. The total amount of water produced in the simulation with 10% clay in the RoM salt pile in the model (one-quarter of the full salt pile) is 119 kg at 460 days. By comparison, the total initial amount of water in the RoM salt with initial saturation of 0.01 and porosity 0.35 is 50.4 kg.

(Insert Fig. 8 and 9)

In Figure 9a, a ring of higher saturation persists outside the boiling region in the case where clay dehydration releases a source of water. The porosity difference between the clay and no clay cases, Figure 9b, shows the slightly greater amount of salt buildup (porosity reduction) in the wetter case with clay dehydration, indicating a bit more heat pipe activity than the case without clay, but clay dehydration does not produce enough water to sustain a vigorous heat pipe as seen in Stauffer et al. (2013). Temperatures are generally cooler for the wetter case, Figure 9c.

The choice of maximum capillary pressure at zero saturation has an effect on the simulations as well. Figure 10 shows the difference in saturation at 460 days between the case with 0.2 MPa and 1 MPa maximum suction. The case with greater suction leads to reduced saturation in the intact salt below the crushed salt pile, slightly increased saturation in the intact salt of the drift ceiling, and increased saturation in the halo outside the boiling front. However, the greater saturation in the crushed salt pile and increased suction are still not enough to drive a vigorous heat pipe in this case.

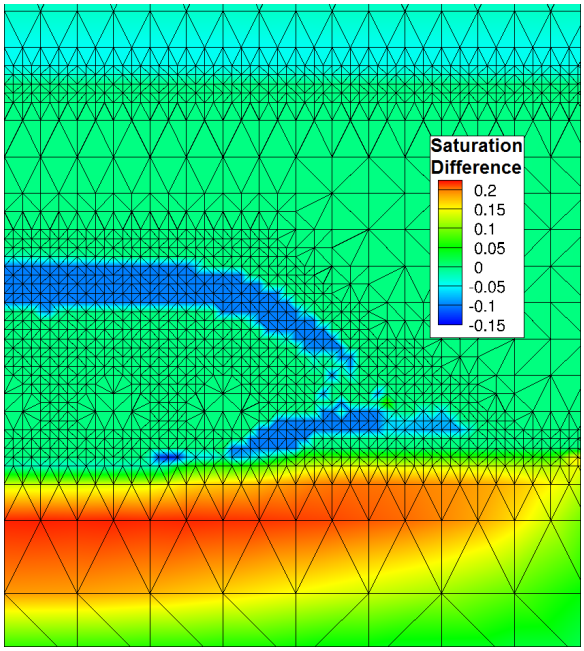

Figure 10: Saturation difference of 0.2 MPa minus 1 MPa maximum suction at 460 days; both cases with 10% clay and initial saturation of 1% in the crushed salt.

Discussion

Concluding Remarks

The interaction between liquid brine flow towards the heat source, establishment of a heat pipe in the mine-run salt backfill, boiling, and vapor condensation leads to changes in porosity, permeability, saturation, thermal conductivity, and rheology of the salt surrounding potential waste canisters. The establishment of a heat pipe depends on waste temperature, moisture availability and mobility (Stauffer et al., 2013). To accurately model the onset and duration of heat pipe activity, fluid fluxes from all sources, including hydrous mineral dehydration, must be quantified. Experimental results from WIPP salt samples show that heating to temperatures of up to 265^{o}C can release over 20% of the mass of accessory (non-halite) mineral material as water. Three steps in a series of dehydration reactions are measured (65, 110, and 265^{o}C) and the amount of water loss associated with each step is averaged from the experimental data into a water source term model in FEHM. The numerical model is then used to predict final temperature, moisture, and porosity after over a year of heating from canisters of high-temperature nuclear waste.

The experimental results indicate that the water content in salt is mainly controlled by the hydrous mineral content, and to a lesser extent, salt brine inclusions. The current clay dehydration model in FEHM does not distinguish between water released by clay dehydration and that produced by other bound water sources such as fluid inclusion migration to a grain boundary. In the future, it is possible that all crushed salt nodes will utilize the “clay dehydration” model to release water from fluid inclusions.

The model currently does not handle clay shrinkage, such as in the seams along the walls of the waste drift, which could lead to enhanced permeability and fluid flux through the damaged rock zone and into the waste drift.

The release of water from clays in the backfill RoM salt, while an important factor in accurately modeling the system, does necessarily not present an obstacle or safety issue for storage in this material. For example, the reduced temperatures around the waste as a result of enhanced heat transfer in a heat pipe are a positive outcome of additional moisture leading to heat pipe activity. Reduced porosities may

provide faster effective "entombment" of the waste in a low-permeability shell. Ultimately, these high-resolution, full-physics short-term predictions of moisture content, temperature, and porosity redistribution in the vicinity of the heated nuclear waste will be used to populate long-term performance assessment models, where the effectiveness of bedded salt formations for isolating nuclear waste can be compared to other materials.

Appendix I References

Beauheim, R. L., & R. M. Roberts (2002). Hydrology and hydraulic properties of a bedded evaporite formation. *Journal of Hydrology*, 259(1), 66-88.

Blanco Martin, L., J. Rutqvist, and J. T. Birkholzer (2013). On the importance of coupled THM processes to predict the long-term response of a generic salt repository for high-level nuclear waste. In *AGU Fall Meeting Abstracts*, vol. 1, p. 1527.

Brady R., C. Herrick, K. Kuhlman, B. Malama, M. Schuhen, and B. Stenson (2013). Sandia Experimental Programs Background and Targeted Activities for Forensic Investigation of Rooms B and A1. NE Milestone M4FT-13SN0818036.

Caporuscio, F.A., H. Boukhalfa, M.C. Cheshire, A.B. Jordan, and M. Ding (2013). Brine migration experimental studies for salt repositories. Los Alamos National Laboratory Document LA-UR-13-27240.

Carter, J.T., Rodwell, P.O., Robinson, B.A., & B. Kehrman (2012). Defense waste salt repository study: Fuel cycle research & development. Report FCRD-UFD-2012-000113, Prepared for U.S. Department of Energy Used Fuel Disposition.

Clayton, D. J. & C. W. Gable (2009). 3-D Thermal Analyses of High Level Waste Emplaced in a Generic Salt Repository. Sandia National Laboratories Report SAND2009-0633P. Albuquerque, NM.

Davies, P. B. (1991). Evaluation of the role of threshold pressure in controlling flow of waste-generated gas into bedded salt at the Waste Isolation Pilot Plant. Sandia National Laboratories Report SAND90-3246/UC-721. Albuquerque, NM.

Harp, D.R., P.H. Stauffer, P.K. Mishra, D.G. Levitt, and B.A. Robinson (2014). Modeling of High-Level Nuclear Waste Disposal in a Salt Repository, accepted, *Nuclear Technology*.

Hansen, F. D., & C. D. Leigh (2011). Salt disposal of heat-generating nuclear waste. Sandia National Laboratories Report SAND2011-0161. Albuquerque, NM.

Kuhlman, K. L., & B. Malama (2013). Brine Flow in Heated Geologic Salt. Sandia National Laboratories Report SAND2013-1944. Albuquerque, NM.

Stauffer, P.H., D.R. Harp, A.B. Jordan, Z. Lu, S. Kelkar, Q. Kang, J. Ten Cate, H. Boukhalfa, Y. Labyed, P.W. Reimus, F.A. Caporuscio, T.A. Miller, and B.A. Robinson. 2013. Coupled model for heat and water transport in a high level waste repository in salt. Los Alamos National Laboratory Document LA-UR-13-27584.

Stauffer, P.H., E.M. Kwicklis, M.J. Sully (2008), Modeling evaporation from a non-vegetated lysimeter experiment, LA-UR-08-0481.

Stone, C. M., Holland, J. F., Bean, J. E., & J. G. Arguello (2010). Coupled Thermal-Mechanical Analyses of a Generic Salt Repository for High Level Waste. 44th U.S. Rock Mechanics Symposium and 5th U.S.-Canada Rock Mechanics Symposium, June 27 - 30, 2010, Salt Lake City, UT.

Zyvoloski, G. A., Robinson, B. A., Dash, Z. V., & Trease, L. L. (1999). Summary of the models and methods for the FEHM application—A finite element mass-and heat-transfer code. Los Alamos National Laboratory Report LA-13307-MS, modified 1999. Los Alamos, NM.